Confronting a refined multiscale estimate for the aging basic creep of concrete with a comprehensive experimental database

F. Lavergne, Jean-François Barthélémy

Confronting a refined multiscale estimate for the aging basic creep of concrete with a comprehensive experimental database.

F. Lavergne[a,*], J.-F. Barthélémy[a]

[a] *Cerema, Equipe-projet DIMA, 110 rue de Paris, BP 214, 77487 Provins Cedex, France*

Abstract

A micro-mechanical scheme has been coupled to a hydration model in [1] so as to investigate the instantaneous mechanical properties of a concrete. That scheme is extended to aging linear viscoelasticity so as to estimate the basic creep of concrete. The compliances of the hydrate phases are set according to existing nanoindentation tests. Then, aging is induced by the progressive dissolution of the unhydrated particles and the precipitation of hydrates at the expense of the capillary porosity. Eventually, these new estimates are extensively compared to 380 published experimental results of basic creep tests gathered in the NU database, thus showing that the method is operational, versatile and reasonably accurate. Finally, accounting for the Young modulus at the time of loading by scaling the estimated strains proved a justified and efficient correction.

Keywords:
concrete, composite, creep, database, hydration

Introduction

Understanding the time–dependent strains of concrete is a matter of importance for the long-term operation of prestressed concrete structures such as box girder bridges and containment buildings. In a divide-and-conquer strategy, the time-dependent strains are split into autogenous shrinkage, drying shrinkage, basic creep and creep induced by drying [2, 3, 4]. The present work is devoted to basic creep, that is the creep strain of a concrete sample covered by a watertight lining or exposed to water-saturated fog. This component of the time–dependent strains is important for thick structures drying slowly and high performance concrete, where the early self-desiccation may limit drying-related strains, especially in wet areas. The basic creep is considered to be a material property, independent of the size of the sample, and it is modelled as aging linear viscoelasticity as long as the stress induced by the compressive load does not exceed 45-50% of the compressive strength of the concrete.

Various physical phenomena have been investigated as potential origins of the basic creep of concrete and accounted for in models [5, 6, 7]. These theories share a common feature: the viscoelastic behavior arises from the small scale, which is the C–S–H gel. Recent evidences are brought by minute-long nanoindentation tests, showing that the shear strain rate of C–S–H is related to its packing density and Ca/Si molar ratio [8, 9, 10, 11].

Different methods have been applied to bridge the gap between the nanometric scale of C–S–H and the metric scale of concrete. The first step consists in using the same functions at both scales and various concrete mix proportions. For instance, the non-aging logarithmic trend of strains measured by minute-long nanoindentation creep tests [8, 9, 10, 11] bears a resemblance to the long-term logarithmic trend of basic creep strains introduced in models B3 [12], B4 [13], *fib* Model Code 2010 [14], first suggested on the basis of macroscopic experimental creep tests [15, 16, 17, 18], though the timeframe and stress magnitudes of nanoindentation tests are largely different from those of macroscopic tests. Nevertheless, macroscopic models of concrete creep feature numerous coefficients that are to be adjusted to account for the composition of the concrete (cement content, water-to-cement ratio...) and retrieve valuable estimates of the overall creep strains if sufficiently long creep tests are not available. The solidification theory [5] led to significant improvement owing to its ability to rigorously deal with aging viscoelasticity and account for the effect of the progressive hydration of the cement. Extending this reasoning, homogenization methods are applied to further account for both the volume fractions and mechanical properties of each phases of the

*Corresponding author
Email address: francis.lavergne@cerema.fr (F. Lavergne)
Postprint of Cement & Concrete Research doi.org/10.1016/j.cemconres.2020.106163

concrete modelled as a composite material [19, 20, 21, 22, 23, 24, 1]. Among these methods, micromechanical schemes based on Eshelby's problem rapidly produce estimates of the linear elastic Young modulus of cementitious materials where pores and stiff aggregates are embedded in a cementitious matrix. The extension to non-aging linear viscoelasticity is possible thanks to the Laplace-Carson transform [25, 26]: assuming that the concrete does not age during the test is required, and it is likely correct as short-time tests are considered [27], or if the concrete is loaded a few months after being cast. Furthermore, numerical simulations based on Finite Element Models [28] of the FFT algorithm [29, 30] also offer valuable alternatives at a higher computational cost. More recently, the Eshelby-based micromechanical schemes have been extended to aging linear viscoelasticity, for both spherical inclusions and ellipsoidal inclusions [31, 32, 33, 34]. It is nevertheless required that the volume fraction of each phase must remain constant during the creep test. As a consequence, accounting for the gradual solidification of hydrates in concrete is achieved by introducing multiple phases for the hydrates: each phase solidifies at a given time [35, 36, 37, 38]. This method could roughly be described as an Eshelby-based solidification theory and it will be extensively be applied herein.

A quantitative estimate of the creep strain of a cementitious material likely requires a precise knowledge of the volume fractions of each species along with their compliances or elastic stiffness. The volume fractions can be sourced from a hydration model providing estimates of the capillary porosity, the volumes of unhydrated cement and hydrates as a function of time, i. e. the Powers model. Nevertheless, since creep is mainly attributed to the C–S–H gel, accounting for its volume fraction may result in an improvement. In addition, if the effect of the overall Ca/Si molar ratio of C–S–H is accounted for, the model of creep strain might be successfully applied to cementitious materials containing pozzolanic additions, such as silica fume and fly ash. As a consequence, the hydration model proposed in [1] is considered, as it provides estimates of volume fractions and Ca/Si molar ratios as a function of time, even for cementitious materials containing pozzolanic additions such as silica fumes and fly ash. Lastly, the accuracy of the proposed model is to be appraised by comparing the new estimates to hundreds of experimental measurements gathered in the NU database [39, 13, 40, 41].

1. Aging viscoelasticity of concrete

1.1. Linear aging viscoelastic micromechanical schemes for composite materials

As concrete is presently modeled as an aging linear viscoelastic composite material, the reasoning aiming at estimating the overall creep strain of such a material is to be depicted. To this end, the mean-field homogenization of aging linear viscoelastic composites [31, 32, 33, 34] is briefly recalled. A linear aging viscoelastic material i is such that its strain history $\varepsilon(t)$ is linearly related to its stress history $\sigma(t)$ via its compliance $\mathbb{J}_i(t,t')$:

$$\varepsilon(t) = \int_0^t \mathbb{J}_i(t,t') : d\sigma(t') \tag{1}$$

The strain and the stress are symmetric tensors of order 2 and the Volterra kernel $\mathbb{J}_i(t,t')$ is a tensor of order 4 depending on two times. A tensorial Volterra operator $\overset{\circ}{:}$ is introduced to rewrite the previous equation as $\varepsilon = \mathbb{J}_i \overset{\circ}{:} \sigma$ [42, 31, 32]. Similarly, the relaxation kernel $\mathbb{C}_i = \mathbb{J}_i^{-1^\circ}$ is such that $\sigma = \mathbb{C}_i \overset{\circ}{:} \varepsilon$, whatever the strain history ε is. It also writes $\mathbb{C}_i \overset{\circ}{:} \mathbb{J}_i = H\mathbb{I}$ where H denotes the function of two times $H(t,t') = H(t-t')$, written with the same symbol as the Heaviside function for the sake of convenience, and $\mathbb{I}$ is the unit tensor of order 4.

A composite material made of $N+1$ linear aging viscoelastic phases $\mathbb{C}_i$, $i \in [0..N]$ of volume fractions c_i is considered. The aging linear viscoelastic homogenization problem consists in finding the overall relaxation kernel of the composite material $\mathbb{C}_{hom}$ [42]. As the problem is linear, the mean strain history $<\varepsilon>_i$ in phase i is linearly related to the overall applied mean strain $<\varepsilon>$ through a concentration kernel $\mathbb{A}_i(t,t')$, tensor of order 4 to be computed, such that $<\varepsilon>_i = \mathbb{A}_i \overset{\circ}{:} <\varepsilon>$ [42]. Hence, the mean stress history $<\sigma>_i$ in phase i is such that:

$$<\sigma>_i = \mathbb{C}_i \overset{\circ}{:} <\varepsilon>_i = \mathbb{C}_i \overset{\circ}{:} \mathbb{A}_i \overset{\circ}{:} <\varepsilon> \tag{2}$$

Finally, the overall mean stress history $<\sigma>$ writes:

$$<\sigma> = \sum_{i=0}^{N} c_i \mathbb{C}_i \overset{\circ}{:} \mathbb{A}_i \overset{\circ}{:} <\varepsilon> \tag{3}$$

and the overall relaxation is identified as [42]:

$$\mathbb{C}_o = \sum_{i=0}^{N} c_i \mathbb{C}_i \overset{\circ}{:} \mathbb{A}_i \tag{4}$$

Hence, an homogenization scheme is defined by its concentration tensors $\mathbb{A}_i$, which themselves likely depend on the behaviors, volume fractions and morphologies of the phases. In the solidification theory, all solidifying phases experience the same strain increments: it corresponds to a parallel configuration, deemed Voigt bound for elastic materials. Hence, the localization tensor writes $\mathbb{A}_i = H\mathbb{I}\ \forall i$ and the overall relaxation kernel is computed as a weighted sum of the relaxation kernels of the phases. On the contrary, a serial configuration (elastic Reuss bound) where all phases experience the same stress can be defined. In such a case, the concentration tensor would write $\mathbb{A}_i = \mathbb{J}_i \overset{\circ}{:} (\sum_j c_j \mathbb{J}_j)^{-\mathring{1}}$ and the overall compliance would be a weighted sum of the compliances of the phases.

Aging linear viscoelastic Eshelby-based homogenization schemes are particularly efficient for matrix-inclusions composite materials. These schemes make use of the Eshelby tensor kernel $\mathbb{S}_{r,A}$ of an ellipsoidal inclusion A_i in a reference material $\mathbb{C}_r$ to compute the concentration tensor [31, 32, 33, 34]. Its most general expression [34] involves the Hill tensor $\mathbb{P}_{r,A}$ as $\mathbb{S}_{r,A} = \mathbb{P}_{r,A} \overset{\circ}{:} \mathbb{C}_r$. Simplified expressions are available for spherical inclusions embedded in any reference material [31] or ellipsoidal inclusions embedded in a reference material featuring a time-independent Poisson ratio ($\mathbb{C}_r(t,t') = \mathbb{C}_r\ f(t,t')$, where $f(t,t')$ is a scalar function) [32]. The strain history in a inclusion of material $\mathbb{C}_i$ embedded in a reference material is linearly related to the strain history far from the inclusion ε_r through a tensor kernel $\mathbb{T}_{ir}$ such that $< \varepsilon_i >= \mathbb{T}_{ir} \overset{\circ}{:} \varepsilon_r$. The tensor kernel $\mathbb{T}_{ir}$ writes:

$$\mathbb{T}_{ir} = \left(H\mathbb{I} + \mathbb{S}_{r,A_i} \overset{\circ}{:} \mathbb{C}_r^{-\mathring{1}} \overset{\circ}{:} (\mathbb{C}_i - \mathbb{C}_r) \right)^{-\mathring{1}} \tag{5}$$

For matrix-inclusion materials, the Mori-Tanaka scheme makes use of the matrix $\mathbb{C}_0$ as a reference material, the strain history far from the inclusion being the average strain in the matrix. The aging viscoelastic concentration tensor therefore writes [31, 43]:

$$\begin{array}{rcll} \mathbb{A}_0 & = & \left(c_0 H\mathbb{I} + \sum_{j>0} c_j \mathbb{T}_{j0} \right)^{-\mathring{1}} & \\ \mathbb{A}_i & = & \mathbb{T}_{i0} \overset{\circ}{:} \left(c_0 H\mathbb{I} + \sum_{j>0} c_j \mathbb{T}_{j0} \right)^{-\mathring{1}} & \forall i > 0 \end{array} \tag{6}$$

The self-consistent scheme is preferred for composite materials where no phase can be described as a matrix. In this case, the reference material is the homogenized behavior itself. Hence, the concentration tensor writes [31]:

$$\mathbb{A}_i = \mathbb{T}_{i,hom} \overset{\circ}{:} \left(\sum_j c_j \mathbb{T}_{j,hom} \right)^{-\mathring{1}} \quad \forall i \tag{7}$$

The equation 4 becomes implicit and it is solved by a fixed point iteration, using the relaxation kernel of one of the phases as the starting point. To turn these expressions into a practical homogenization method, time steps are introduced and integrals are computed using a quadrature rule [44, 45, 31, 32]. In this time discretization strategy, strain and stress histories are pictured as vectors and relaxation and compliance kernels become block triangular matrices. The tensor Volterra operators $\overset{\circ}{:}$ become either a matrix-vector product or a matrix-matrix product and the inversion $\mathbb{C}^{-\mathring{1}}$ maps to the inversion of a matrix.

At this point, any micromechanical scheme aiming at estimating the elastic strain of concrete as a composite material can be promptly turned into a micromechanical scheme devoted to basic creep strains, as long as the changes of the microstructure occurring after loading are neglected, a limitation removed in the next section.

1.2. Accounting for dissolution and solidification

The hydration model [1] produces estimates for the volume fraction of each phase of the concrete in the course of hydration, at each time t_i, $i \in [0..N]$. The elastic homogenization scheme described in [23, 1], features 4 scales from the larger to the lower: the scale of concrete, that of cement paste, that of hydrate foam and that of hydrate. The changes of the volume fractions of each phases must be accounted for as performed in [35, 36, 37, 38] to model the creep strain induced by the dissolution of load-bearing reactants (fig. 1.2). The resulting scheme is depicted in figure 1.1. Compared to the elastic scheme, it features additional phases

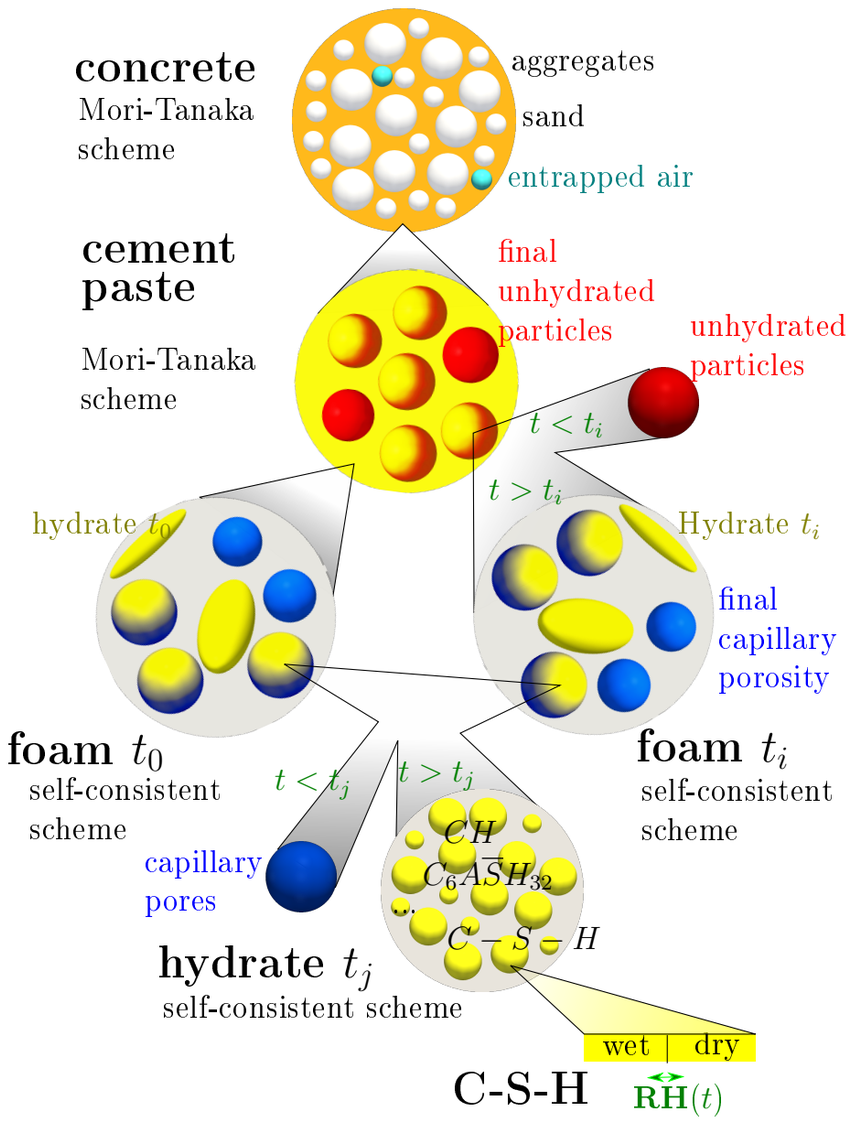

Figure 1.1: The multiscale homogenization scheme is adapted to viscoelasticity. At the scale of the cement paste, spheres graded from red to yellow describes the shift from unhydrated particles to hydrate foam. Similarly, at the scale of the hydrate foams, spheres graded from blue to yellow describes the filling of capillary pores by hydrates.

describing the replacement of unhydrated particles by newly-formed hydrate foam and the filling of the capillary pores of the hydrate foams by newly-formed hydrates.

At the scale of the hydrate foam, the capillary porosity is gradually filled by the hydrates. It is assumed that the hydrate foam is stress free as it precipitates. Consequently, the relaxation tensor $\mathbb{C}_{i:p\to h}$ of a pore filled by hydrates at time t_i writes:

$$\mathbb{C}_{i:p\to h}(t,t') = H(t'-t_i)\ \mathbb{C}_{i:h}(t,t') \tag{8}$$

where $\mathbb{C}_{i:h}$ is the relaxation tensor of the hydrates formed at time t_i. This tensor is itself the result of an homogenization step, where the volume fraction of C–S–H is accounted for. At the scale of the cement paste, the unhydrated particles are gradually replaced by the hydrate foam. It is assumed that the dissolution of the cement particle and the formation of the hydrate foam result in a dissipation of the elastic energy stored in the cement particles. Consequently, the relaxation tensor $\mathbb{C}_{i:u\to f}$ of an unhydrated particle replaced by hydrate foam at time t_i writes:

$$\mathbb{C}_{i:u\to f}(t,t') = (1-H(t-t_i))\ \mathbb{C}_u + H(t'-t_i)\ \mathbb{C}_{i:f}(t,t') \tag{9}$$

The first term using the elasticity tensor of the unhydrated particles $\mathbb{C}_u$ describes the dissolution of the unhydrated particles and the second term using the relaxation tensor of the

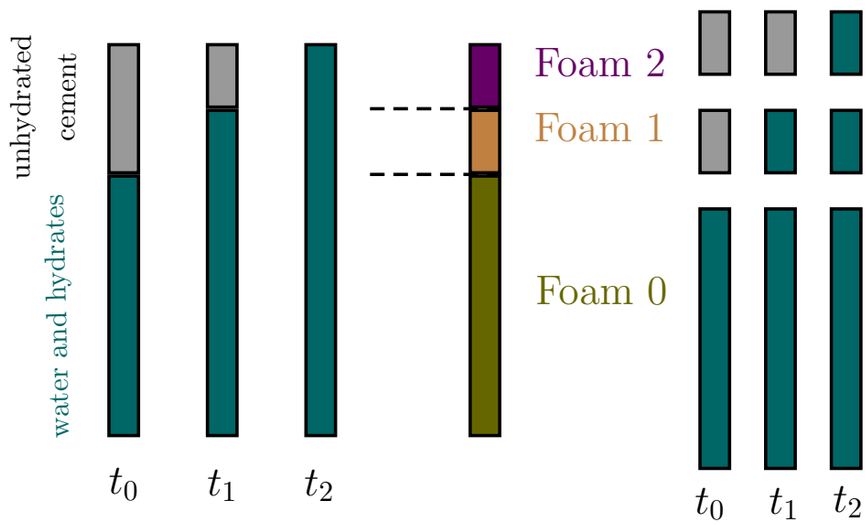

Figure 1.2: Instead of accounting for time-dependent volume fractions of unhydrated cement and hydrate foam, phases of fixed volume fractions accounting for dissolution of cement and the formation of the foam are introduced [35]. The number of these new phases is equal to the number of time steps.

hydrate foam $\mathbb{C}_{i:f}(t,t')$ describes the stress-free precipitation of the hydrate foam on the interval $]t_{i-1},t_i]$.

Accounting for the changes of volume fractions as performed in [35] multiplies the number of phases in the multiscale micromechanical schemes (fig. 1.2). Indeed, a phase at a given scale is characterized by its composition, its time of formation and the history of its solidification. As a result, there are N different compliances for the hydrate foams, depending on when it is formed. Furthermore, the foam formed at time t_i is made of $N-i+1$ hydrates $h_{i,j}$, $j \in [i..N]$ describing its progressive solidification. Its additional capillary porosity is always equal to the overall capillary porosity: this assumption dictates the volume fraction of hydrates $h_{i,j}$ in the foam i. Moreover, it can reasonably be assumed that the chemical composition of the hydrate only depends on the time of its formation j and remains independent from the time of the formation of the foam i that contains it. Therefore, the index j being set, the chemical composition $[c]_j(t_k)$ $(k \geq j)$ of all hydrates $h_{i,j}$ such that $i \leq j$ are similar. This assumption also limits the number of hydrate mixes to N, thus easing the computations.

On the one hand, to remain consistent with existing micromechanical scheme in the range of elasticity, it can be assumed that the whole hydrate foam remains uniform at all time: $[c]_j(t_k) = [c](t_k) \forall k \geq j$. For instance, in the case of a mix containing fly ash, the pozzolanic reaction could lead to a consumption of Porlandite after a few weeks. Nevertheless, the uniformity would imply that Portlandite is being precipitated in the newly formed hydrates, while the dissolution rate of Portlandite in old hydrates would be raised: some Portlandite would move from the old hydrates to the new ones by a dissolution-precipitation phenomenon, thus leading to an additional creep strain. On the other hand, the composition $[c]_j(t_k)$ can be described according to a last-in first-out (LIFO) order (fig. 1.3), limiting the mechanical effect of dissolution-precipitation to the minimum. As a result, the Portlandite that is dissolved is the last that have been formed. It is consistent with the view that Portlandite is formed as crystals, the outer layer or the younger small crystals being dissolved first to provide calcium to the pozzolanic reactions. The same order is applied to ettringite, which turns into monosulphoaluminate or monocarboaluminate depending on the temperature and the availability of calcite. The LIFO order introduced and applied in the present article reduces the relaxation induced by dilution-precipitation mechanisms to the minimum whenever the dissolution of a hydrate is modelled.

1.3. The compliance of the cementitious phases

The compliance of the individual phases of the hydrates can be identified by performing nanoindentation lasting less than 5 minutes [9]. The preferred base function to be adjusted to the measured time-dependent strain is a logarithm, thus :

$$\mathbb{J}(t,t') = \mathbb{C}^{-1}H(t-t') + \mathbb{D}\ln\left(1+\frac{t-t'}{\tau}\right)H(t-t') \tag{10}$$

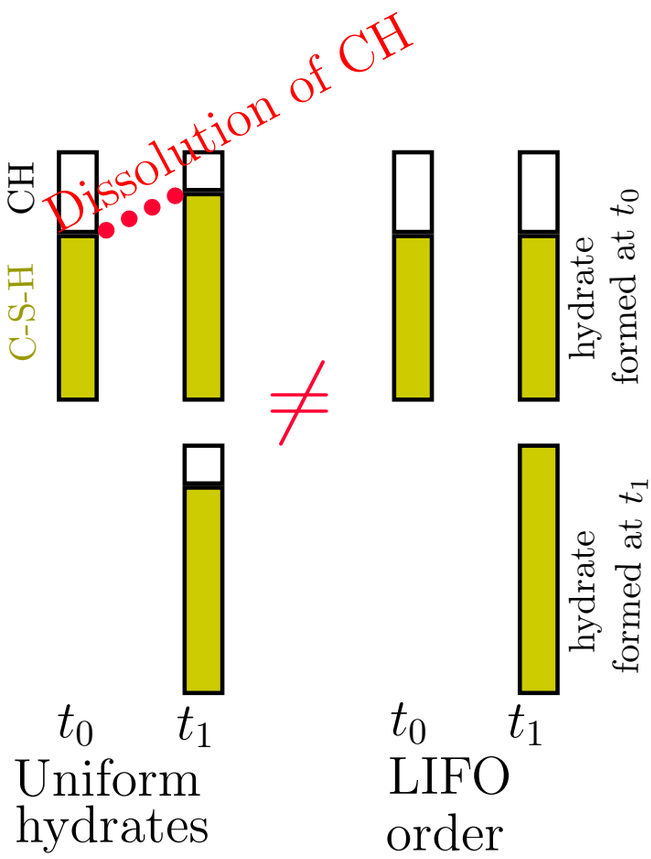

Figure 1.3: A situation where all the Portlandite (CH) produced by hydration reactions is consumed by pozzolanic reactions on the time step $[t_0; t_1]$. Assuming the hydrates to be of uniform chemical composition (left) induce dissolution of Portlandite in existing hydrates. On the contrary, the LIFO order (right) ensures that Portlandite is dissolved if and only if the overall Portlandite content decreases.

where the elastic stiffness $\mathbb{C}$ and the creep compliance $\mathbb{D}$ are isotropic tensors to be adjusted. The Poisson ratio of the tensor $\mathbb{D}$ is often assumed to be similar to that of $\mathbb{C}$ so that the instantaneous Young modulus E of tensor $\mathbb{C}$, the Young modulus $E_{\mathbb{D}}$ of stiffness tensor $\mathbb{D}^{-1}$, the characteristic time τ and the Poisson ratio are the four scalar parameters describing the compliance of the phase. The characteristic time τ features a median value of 0.7s [9]. First, the characteristic time is not as important as for a Kelvin chain since the long-term strain rate does not depend on it. Furthermore, upscaling the estimated long-term creep rate to the macroscopic scale where experiments last months or years has been achieved by mean of micromechanics [9]. Indeed, as long as non-aging viscoelasticity is considered, using the Laplace-Carson transform and the corresponding final value theorem, it has been shown that the logarithmic trend is not altered by mean field schemes [9]. Lastly, the similarity to the creep of granular materials suggests a granular origin to the creep of C–S–H [9], thus providing a physical foundation supporting the use of this trend. Finally, the long-term logarithmic trend is consistent with experimental measurements performed at the macroscopic scale [15, 16, 17, 18] and introduced in many up-to-date standards and models to estimate the basic creep strain of cementitious materials [12, 13, 14].

1.3.1. From contact creep compliance to the creep compliance of the indented material

The estimated creep compliance measured by nanoindentation measurements on cement pastes likely corresponds to the non-aging compliances of pure phases if the applied load is about 0.5–2mN. Indeed, it corresponds to indentation depths h_{max} lower than 200nm, a scale where the individual phases such as Portlandite are visible on SEM images [46, 8, 47]. Performing microindentation tests at loads greater than 5N on reconstituted pure-phase compacts also provides a sound base for setting the compliance of pure phases [11, 10]. The temperature and relative humidity during the creep test likely influence the creep rate. Nevertheless, these environmental parameters are not discussed in [8, 9], where room temperature and low relative humidity can be assumed. For instance, the numerous tests of Zhang [10] explore the effect of the relative humidity on the compliance of C–S–H featuring a Ca/Si ratio of 1.4 and Portlandite. Both the local chemical composition and the mechanical properties

can be measured by combining the nanoindentation and Scanning Electron Microscopy with energy-dispersive X-ray spectroscopy (SEM-EDS) [48, 47].

The contact creep modulus and indentation modulus can also be measured by performing microindentation tests on reconstituted pure phases[10, 11]. Nevertheless, reconstituted compacts of pure phase features an additional porosity and the density of the indented pure phase can differ from that of the phases considered in the homogenization process. For instance, the Cpt-CSH compact of Zhang [10] features a porosity of $\phi' = 20.8\%$ if the solid density of C–S–H is 2.21g/cm^3. Then, the saturated density of the indented sample is about 1.96 g/cm^3. The C–S–H gel considered in the proposed homogenization process features a saturated density of 2.1 g/cm^3. As a result, the indented Cpt-CSH compact can be pictured as a porous C–S–H featuring a porosity of $\phi = 13.6\%$. Consequently, the stiffness of the C–S–H could be identified starting from those measured on Cpt-CSH using a Mori-Tanaka scheme or a self-consistent scheme. The aspect ratio of the C–S–H or the considered micromechanical scheme do not largely influence the identified properties of C–S–H since the porosity $\phi = 13.6\%$ is very low.

Nevertheless, if the viscoelastic Poisson ratio is supposed to be time-independent, the indentation modulus of the compact must vary directly with its contact creep modulus and the characteristic time must be independent from the porosity, thus avoiding the need for an homogenization scheme. Indeed, the morphology of the porous network in the compact would affect both in the same way. It could be proved by applying the Laplace-Carson transform for non-aging linear viscoelastic material [30], or more comprehensively for any heterogeneous microstructures where an aging viscoelastic material, a porous network and rigid perfectly adhesive inclusions are mixed. The reasoning proposed in [49] is followed. Indeed, let $\mathbb{J}(t,t') = \mathbb{C}^{-1}f(t,t')$ be the compliance of the solid skeleton and $\varepsilon(x,t')$ be the local elastic strain due to a loading performed at t' according to homogeneous stress boundary conditions. If a creep test is performed by maintaining this loading, the strain at any time $t \geq t'$ clearly writes $\varepsilon(x,t) = \varepsilon(x,t')f(t,t')/f(t',t')$ and the stress field remains similar to its value right after the loading. The rotation field and the relative displacements are also scaled by the same factor. As a result, the overall compliance, obtaining by averaging $\varepsilon(x,t)$, is also of the form $\mathbb{J}_{compact}(t,t') = \mathbb{C}^{-1}_{compact}f(t,t')$, relying on the same function $f(t,t')$. Moreover, the morphology of the porous network only affects $\mathbb{C}^{-1}_{compact}$. The reasoning can be extended by superposition to combinations of sustained displacements boundary conditions and sustained loadings on viscoelastic structures (fig. 1.4). Indeed, the notion of effective modulus, widely applied to design structures, becomes rigorous within this scope of time-independent Poisson ratio.

The present reasoning bears some important consequences regarding the effect of the size distribution of aggregates on the time-dependent strains of concrete. Indeed, if the aggregates are infinitely rigid and perfectly adhesive to the cement paste, the volume fraction, size distribution and shapes of the aggregates and pores must affect the elastic Young modulus and the viscoelastic compliance in the same way. It is also the case if the aggregates are viscoelastic with a time-independent Poisson ratio and the same function $f(t,t')$ as the paste or if the interface is ruled by an ageing linear viscoelastic law of compliance also written as a constant tensor $\mathbb{K}$ times $f(t,t')$: the case of local debonding ($\mathbb{K} = 0$) is also analytically solved. Nevertheless, some configurations of interest are not covered by this analytic reasoning. By means of 3D numerical simulations, it is proposed in [30, 32] that it can be considered as valid for finite contrasts of stiffness and nearly spherical aggregates but recent numerical simulations suggest that extended aggregate size distributions [50] or non-convex aggregates [51] induce lower creep strains . By applying mean-field schemes, it has been estimated in [33] that elongated elastic steel fibers are more efficient at mitigating the long-term creep strains than at reducing the elastic strains. Finally, extending the validity range to any morphology and any finite contrast is clearly incorrect. Indeed, the longitudinal compliance of a composite materials made of successive layers of a soft elastic material and stiff viscoelastic material does not vary directly with the compliance of the viscoelastic material.

Furthermore, if clear experimental evidences showed that the indentation modulus of the compact does not vary directly with its contact creep modulus (as suggested for the different phases of a cement paste by fitted trends in [52, 11]) or if the characteristic time were not left unchanged by compaction, either the assumption of the logarithmic trend, that of a time-independent Poisson ratio, that of an homogeneous skeleton featuring a time-independent morphology, or that of linear viscoelasticity would have to be questioned.

The characteristic time $\tau = 0.7 - 3s$ identified during indentation tests [52, 11, 10] does not correspond to the characteristic time of concrete creep measured on full-scale samples (in

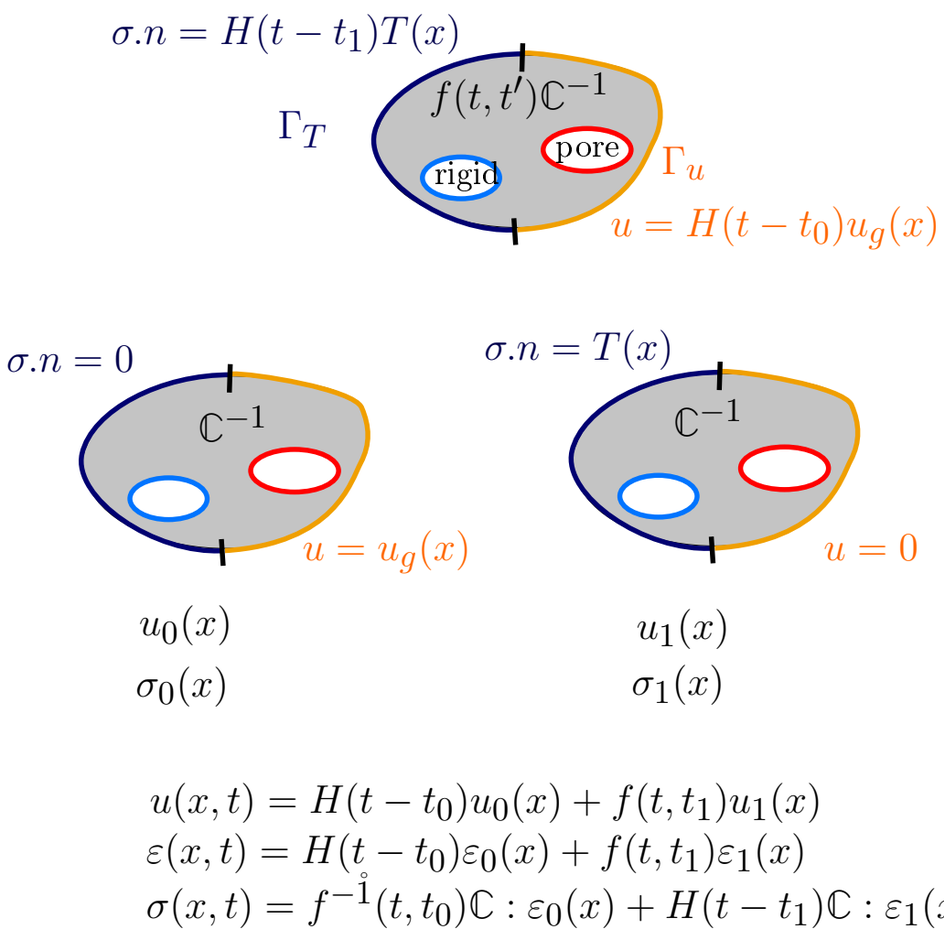

$$u(x,t) = H(t-t_0)u_0(x) + f(t,t_1)u_1(x)$$
$$\varepsilon(x,t) = H(t-t_0)\varepsilon_0(x) + f(t,t_1)\varepsilon_1(x)$$
$$\sigma(x,t) = \mathring{f^{-1}}(t,t_0)\mathbb{C} : \varepsilon_0(x) + H(t-t_1)\mathbb{C} : \varepsilon_1(x)$$

Figure 1.4: On top, sustained displacements boundary conditions $u_g(x)$ and sustained loadings $T(x)$ are applied to the heterogeneous aging viscoelastic structure featuring a time-independent Poisson ratio $\mathbb{J}(x,t,t') = \mathbb{C}^{-1}(x)f(t,t')$. Rigid inclusions and pores are embedded in that matrix. Its displacement $u(x,t)$ is a linear combination of the solutions to the two elastic problems in the middle [49]. $\mathring{f^{-1}}$ refers to the inverse of function f with respect to the Volterra operator.

phase	experimental conditions	$E_{\mathbb{D}}/E$	source	comments
C–S–H		5.1	[9]	LD: 5.0, HD:5.2
CH	11%RH	21	[11]	
1.4nm Tobermorite	11%RH	7.2	[11]	
Jennite	11%RH	7.1	[11]	
C–S–H	11%RH	9.2	[11]	C/S=0.6
C–S–H	11%RH	5.3	[11]	C/S=0.8
C–S–H	11%RH	5.3	[11]	C/S=1.0
C–S–H	11%RH	4.4	[11]	C/S=1.2
C–S–H	11%RH	5.7	[11]	C/S=1.5
$C\bar{S}H_2$	11%RH	20	[11]	
Ettringite	11%RH	11	[11]	Ettringite
C–S–H	23°C, 100%RH	2.6	[10]	Cpt-CSH C/S=1.5 ($\nu = 0.24$)
C–S–H	23°C, 94%RH	1.6	[10]	Cpt-CSH C/S=1.5
C–S–H	23°C, 75%RH	2.0	[10]	Cpt-CSH C/S=1.5
C–S–H	23°C, 54%RH	2.5	[10]	Cpt-CSH C/S=1.5
C–S–H	23°C, 33%RH	3.7	[10]	Cpt-CSH C/S=1.5
C–S–H	23°C, 11%RH	5.3	[10]	Cpt-CSH C/S=1.5

Table 1.1: Ratios between the Young modulus of the logarithmic trend $E_{\mathbb{D}}$ and the elastic modulus E are identified on indentation results stemming from different sources, under the assumption of a time-independent Poisson ratio.

days or weeks) [9, 10]. For instance, the characteristic time for a cement paste is identified to be 3.3 days in [10, 50], it is valued at more than 10 days for concrete loaded after 100 days [17]. Moreover, the change of the characteristic time can hardly be fully attributed to the change of scale as multiplying by 10 the indentation depth leads to comparable indentation characteristic time[9]. Similarly, it has been shown that the characteristic time is likely independent from the strain level by using indentation probes featuring different shapes [9]. On the contrary, the difference of characteristic time might be attributed to the magnitude of stress [9], which are similar to the indentation hardness in the case of an indentation test. In addition, a backward identification of the characteristic time for the creep of C–S–H using full-scale measurements coupled to a non-aging micromechanical scheme delivered values $\tau = 0.278$h, $\tau = 0.75$h and $\tau = 4$h [26] and the characteristic time λ_0 in the non-aging solidifying compliance of the B3 model applied to C–S–H is similar to that of cement paste and concrete, estimated to be 1 day [29]. Indeed, a characteristic time of 1 day has been implicitly adopted in logarithmic trends of creep strain for decades [15, 16]. Furthermore, the characteristic time can be described as an increasing function of the loading time t' [26, 17, 18] to account for aging at the structural scale. For instance, the characteristic time $\tau(\text{days}) = 1/(30/t'_{adj} + 0.0035)^2$ of the *fib* model code 2010 remains in the wide interval [24s, 81632days] since the adjusted age at loading t'_{adj} cannot be lower than 0.5 days. Nevertheless, the difference of characteristic time did not arise as a problem in the aging viscoelastic simulations of cement paste [28], where the characteristic time coming from nanoindentation measurements is used at the scale of C–S–H.

Lastly, recent molecular models of the creep of C–S–H [53] compliant with its nanogranular origin [52] offer an opportunity for understanding this difference of characteristic time. Indeed, the creep strain is not computed as function of time, but as a function of perturbation cycles [53, 7]. It is observed that the creep rate varies indirectly with the number of perturbation cycles in the long run. Hence, it can be assumed that the frequency or level of perturbations are much higher during indentation tests than during full-scale tests to resolve the difference of characteristic time. Finally, the creep strain is accelerated by a time-perturbation shift, similar to the time-temperature shift encountered as the creep of plastic materials is studied.

On the base of the nanoindentation tests gathered in table 1.1, the compliance of CSH is set as a function of the C/S ratio. Its basic creep strain varies directly with the relative humidity RH at loading as observed on pre-dried cement pastes [54, 55, 56, 3, 57, 58], though the identified $\frac{E_{\mathbb{D}}}{E}$ on the base of nanoindentation tests of [10] (Tab. 1.1) do not perfectly follow this trend:

$$\frac{E_{\mathbb{D}}}{E} = 1.2(14(\text{C/S})^2 - 33\text{C/S} + 24)\frac{0.11}{RH} \tag{11}$$

Hence, the compliance of C-S-H computed according to the previous equation features a

maximum at C/S=1.18, where $E_{\mathbb{D}}/E = 5.5$, compared to $E_{\mathbb{D}}/E = 10.$ at C/S=1.7, RH=11%. A 1.2 corrective factor has been added in equation 11 to retrieve the magnitude of long term trend of C–S-H creep identified in [26, 33] (fig. 2.3). Similarly, the characteristic time τ is set to 0.5 days for macroscopic creep tests. The elastic Young modulus of $E = 25.$ GPa and Poisson ratio of 0.24 considered in [1] for the $C_{1.7}SH$ and $C_{1.1}SH$ of respective molar volume 108.3cm^3/mol and 101cm^3/mol are combined to equations (11) and (10) so as to estimate the compliance of C-S-H gel. The compliances of monosulphoaluminate and monocarboaluminate are also assumed to be logarithmic, the $E_{\mathbb{D}}/E$ ratio being set equal to that of a C-S-H of C/S ratio 1.7, following evidences in [48]. Furthermore, both Portland cements of different types and high-alumina cement lead to sensibly the same creep if comparable strength at the time of loading are considered [59]. Given the limited number of experimental evidences on the subject, further investigations could confirm or discard the proposed trends. Nevertheless, the proposed trends can easily be adapted to comply with future experimental evidences.

1.3.2. Accounting for variable relative humidity during creep tests

Equation (11) does not specify when the relative humidity must be evaluated and it could have been a problem for sealed high performance concrete or drying structures. Nevertheless, variation of internal relative humidity are rarely accounted for in basic creep models because its origin, the self-desiccation induced by hydration, limits its amplitude. Indeed, the relative humidity remains in the range 80%-100%. Nevertheless, an innovative method is presently introduced in the hope for paving the way of future models of drying creep.

On the one hand, using the relative humidity at the moment of loading t' in equation (11) would induce creep strains independent from the changes of relative humidity occurring after loading. In addition, loading later would result in larger creep strain at time t in case of re-wetting, thus breaching the thermodynamic requirements for a correct compliance. On the other hand, using the relative humidity at time t would not account for the moment of drying, not to mention that a drying structure could feature decreasing creep strains. As a clever alternative, it is often considered that the relative humidity at time t affects the creep rate at time t [58, 60]:

$$\frac{\partial J}{\partial t}(t,t') = f(RH(t))\frac{\partial J_{RH=100\%}}{\partial t}(t,t') \tag{12}$$

Such an expression bears some similarities with the solidification creep: the function $f(RH(t))$ is similar to the inverse of the load-bearing fraction of solidified material. Hence using $f(RH(t)) = RH(t)$ as in [58, 60] or $f(RH(t)) = 1/g(RH(t))$ where g is a decreasing function [50] corresponds to an increase of the volume fraction of load-bearing solidified material as long as drying is considered. As a consequence, this compliance alone does not induce a significant drying creep and a supplementary drying creep compliance, or a stress-induced shrinkage [61] where the creep rate varies directly the absolute value of the rate of the relative humidity [58, 60, 50] is added to model drying creep.

Nevertheless, developing the analogy to the solidification theory provides a straightforward way to define a necessary drying creep. It is proposed that the C–S–H features two kind of links: wet ones and dry ones. The wet links, or creep sites, creep more than the dry links. The proportion of wet links $c_{wet}(RH(t)) \in [0,1]$ must depend on the relative humidity so as to comply with the observed creep strain at fixed relative humidity. As the relative humidity diminishes, some wet links must be broken to form dry links, thus generating drying creep. The proposed description can be qualified as phenomenological since it does not stem from a particular physical phenomenon. Indeed, it would obviously comply with a dissolution-precipitation mechanism. On the contrary, the cursor $c_{wet}(RH(t))$ could have been driven either by microdiffusion [61] or by a relaxation of a microprestress [6]. Furthermore, the dry C–S–H could have been pictured as a densified C–S–H and the densification process could be described as consolidation, a collapse of C–S–H layers [62] or a reorientation of globules [63].

If the links are assumed to be parallel, the overall relaxation kernel of C–S–H $\mathbb{C}(t,t')$ can be written within the framework of the solidification theory. The fractions of wet and dry links remaining undamaged between time t' and t respectively are $\min_{\tau\in[t,t']}(c_{wet}(RH(\tau)))$ and $1 - \max_{\tau\in[t,t']}(c_{wet}(RH(\tau)))$. As a consequence, the relaxation kernel writes:

$$\mathbb{C}(t,t') = \left[1 - \max_{\tau\in[t',t]}(c_{wet}(RH(\tau)))\right]\mathbb{C}_{dry}(t,t') + \left[\min_{\tau\in[t',t]}(c_{wet}(RH(\tau)))\right]\mathbb{C}_{wet}(t,t') \tag{13}$$

where $\mathbb{C}_{dry}(t,t')$ and $\mathbb{C}_{wet}(t,t')$ are the relaxation kernels of the dry and wet links. These kernels are set according to the equations 10 and 11. Hence, that of a wet links corresponds to RH=100% and that of the dry links is purely elastic (RH=0%).

During a drying relaxation test, these new dry links remain unstressed and the breakage of wet links results in a drying relaxation. During a drying creep test, the breakage of the wet link induces an additional creep strain: a drying creep would occur. Upon re-wetting, some dry links are broken to form wet links and a drying creep is to occur as well. But it proves much smaller than the actual drying creep strain in cementitious materials [57] as the estimated creep strain of a drying C–S–H does not significantly exceed that of a saturated C–S–H. Furthermore, setting the dry C–S–H as purely elastic alters the logarithmic long-term trend of creep strains. It is due to the parallel geometry presently investigated: dissolving a small fraction of wet links thus induces a small relaxation. To recover a valuable estimate of the drying creep strain, it is therefore necessary to introduce another softer geometry. Hence, the wet links and dry links are connected in a series connection and their compliances are added instead of their relaxation. The compliance of the C–S–H then writes:

$$\mathbb{J}(t,t') = \min_{\tau\in[t',t]}(c_{wet}(RH(\tau)))\mathbb{J}_{wet}(t,t')+(1-\max_{\tau\in[t',t]}(c_{wet}(RH(\tau))))\mathbb{J}_{dry}(t,t')+\int_{\min(c_{wet}(RH(\tau)))}^{\max(c_{wet}(RH(\tau)))}\mathbb{J}_c(t,t')\mathrm{d}c \tag{14}$$

The compliance $\mathbb{J}_c$ of the phase of cursor value c turns from wet to dry or from dry to wet each time the cursor $c_{wet}(RH(\tau))$ crosses the cursor value c. For instance, if this phase turns from wet to dry at time $t_c^{w\to d}$, its compliance writes:

$$\begin{array}{rcll}\mathbb{J}_c(t,t') & = & \mathbb{J}_{wet}(t,t') & t < t_c^{w\to d} \\ & = & \mathbb{J}_{wet}(t_c^{w\to d},t') + \beta\mathbb{C}^{-1} + \mathbb{J}_{dry}(t,t_c^{w\to d}) & t' < t_c^{w\to d} < t \\ & = & \mathbb{J}_{dry}(t,t') & t_c^{w\to d} < t'\end{array} \tag{15}$$

This compliance is obtained by following the process described in figure 1.5. First, at time $t_{w\to d}$, a rigid shunt is placed parallel to the phase c, preventing any displacement as an inertia would do. Then, the wet C–S–H is dissolved: the stress is entirely transferred to the shunt. Then, the new dry C–S–H is precipitated stress-free. As the rigid shunt is removed, the stress is transferred to the dry C–S–H, thus inducing an immediate additional elastic strain as a creep test is considered. If a relaxation test is performed on the changing element alone, the relaxation is complete whenever the strain is applied prior to dissolution. The additional compliance $\beta\mathbb{C}^{-1}H(t-t_{w\to d})H(t_{w\to d}-t')$ corresponds to multiple instantaneous sequences of bond being formed, elastically strained and broken. Finally, the scalar parameter β drives the amplitude of drying creep strains.

As the basic creep strain of C–S–H are assumed to vary directly with the relative humidity at loading and given the serial configuration, the proportion of wet $c_{wet}(RH(t)) = RH(t)$ is set equal to the relative humidity. The parameter β is set to 30 to retrieve a significant drying creep. The series connection between wet and dry C–S–H implies that the wet C–S–H may turn into dry C–S–H without experiencing a change of stress as a stable loaded C–S–H foam is dried. In particular, it is not consistent with a physical description limited to a slow dissolution-precipitation mechanism where the new phase would be required to be stress-free right after precipitation. Finally, the multiscale scheme nevertheless ensures that both wet and dry C–S–H being part of newly precipitated hydrate foam are stress-free as precipitation occurs.

1.4. Numerical implementation

The numerical implementation is identical to that introduced in [38]: time is discretized into time steps $0 < t_0 <, ..., < t_n$ and a quadrature rule is used to approximate integrals and solve the Volterra equation. The strain history and the relaxation function are approximated as piecewise linear functions, thus turning the strain history into a vector and the relaxation kernel into a matrix. The stress history $\sigma = \mathbb{C}\overset{\circ}{:}\varepsilon$ is estimated by trapezoidal approximation:

$$\sigma(t_l) = \mathbb{C}(t_l,t_0) : \varepsilon(t_0) + \sum_{m=0}^{l-1}\frac{1}{2}(\mathbb{C}(t_l,t_m)+\mathbb{C}(t_l,t_{m+1})) : (\varepsilon(t_{m+1})-\varepsilon(t_m)) \tag{16}$$

On the one hand, accounting for the dissolution of a phase is straightforward. Indeed, if the dissolution occurs at time $t_d \in]t_k, t_{k+1}[$, the rows $0..k$ of the matrix are left unchanged because the stress history is not influenced by the dissolution. On the contrary, all rows $k+1..n$ must be zeroed, because the stress must be null after dissolution.

On the other hand, accounting for the continuous precipitation on the time step requires some attention. As performed in [38], the gradual precipitation can be modelled as step-wise precipitations where each phase massively precipitates at time t_i between the numerical time

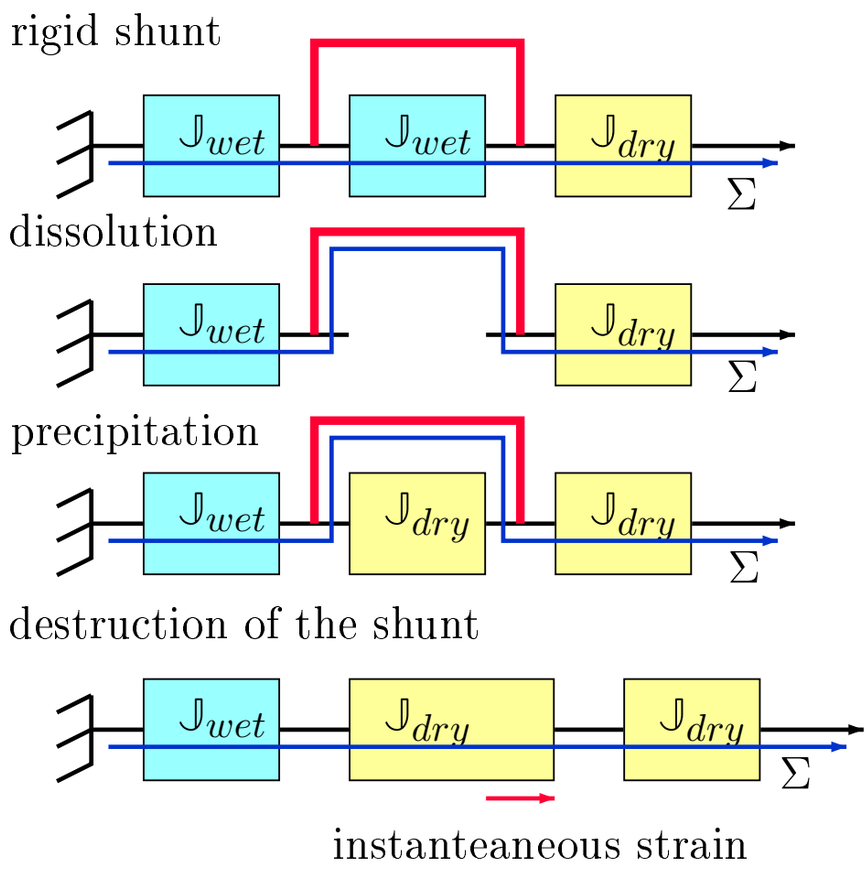

Figure 1.5: The 4-step process defining the serial solidification compliance. This process induces an additional instantaneous strain in case of a creep test.

step t_k and t_{k+1}. Nevertheless, the actual value of t_i does not influence the matrix obtained by applying equation 16, which becomes:

$$\sigma(t_l) = \frac{1}{2}\mathbb{C}(t_l, t_{k+1}) : (\varepsilon(t_{k+1}) - \varepsilon(t_k)) + \sum_{m=k+1}^{l-1} \frac{1}{2}(\mathbb{C}(t_l, t_m) + \mathbb{C}(t_l, t_{m+1})) : (\varepsilon(t_{m+1}) - \varepsilon(t_m)) \tag{17}$$

An applied strain rate on the time step $[t_k, t_{k+1}]$ is therefore handled as if it was a relaxation test of half the magnitude applied a time t_{k+1}. If the actual t_i is close to t_{k+1}^-, the regular strain increase occurs before precipitation and the stress should be null. On the contrary, if t_i is close to t_k^+, the regular strain increase occurs after precipitation and the stress induced by the applied strain rate, approximated according to the quadrature rule, would actually write:

$$\sigma(t_l) = \frac{1}{2}(\mathbb{C}(t_l, t_k^+) + \mathbb{C}(t_l, t_{k+1}))(\varepsilon(t_{k+1}) - \varepsilon(t_k)) \tag{18}$$

The use of equation 16 regardless of the actual value of t_i can therefore be considered as a regularization and improves the modelling of gradually precipitating materials.

To improve the consistency of the regularization, the integration of the Volterra equation can be modified by accounting for the progressive precipitation of the material on the time step. Assuming a parallel geometry as in the solidification theory and that the volume fraction of precipitated material at time $t_k < t' < t_{k+1}$ is $(t' - t_k)/(t_{k+1} - t_k)$, the overall relaxation of the precipitating material at time $t \geq t_{k+1}$ writes:

$$\mathbb{C}_p(t, t') = \frac{t' - t_k}{t_{k+1} - t_k}\left[\mathbb{C}(t, t_k^+) + \frac{t' - t_k}{t_{k+1} - t_k}(\mathbb{C}(t, t_{k+1}) - \mathbb{C}(t, t_k))\right] \tag{19}$$

A regular strain rate $\varepsilon(t') = \varepsilon(t_k) + [(t' - t_k)/(t_{k+1} - t_k)](\varepsilon(t_{k+1}) - \varepsilon(t_k))$ limited to the time step would therefore result in the following stress response at all time $t_l \geq t_{k+1}$:

$$\begin{array}{rcl} \sigma(t_l) & = & \int_{t_k}^{t_{k+1}} \mathbb{C}_p(t_l, t') \frac{\varepsilon(t_{k+1}) - \varepsilon(t_k)}{t_{k+1} - t_k} dt' \\ \sigma(t_l) & = & (\frac{1}{6}\mathbb{C}(t_l, t_k) + \frac{1}{3}\mathbb{C}(t_l, t_{k+1}))(\varepsilon(t_{k+1}) - \varepsilon(t_k)) \end{array} \tag{20}$$

Therefore, the implicit regularization of the massive precipitation performed in [38] can also be viewed as a progressive precipitation, as long as $\mathbb{C}(t_l, t_k) \approx \mathbb{C}(t_l, t_{k+1})$. This limitation is

obviously satisfied by elastic non-aging materials, or in case of short time steps. In addition, due to thermodynamic laws, $\mathbb{C}(t_l, t_k) \leq \mathbb{C}(t_l, t_{k+1})$ (where $\leq$ means that the difference is positive semi definite) since $t_{k+1} \geq t_k$. Hence, as long as parallel progressive precipitation and piecewise affine functions are considered, the numerical implementation of precipitation introduced in [38] is accurate. It is also rigorously applied to describe the progressive precipitation of inclusion phases in Eshelby-based micromechanical schemes because the inclusion phases are always surrounded by a matrix that limits the effect of dissolution-precipitation.

Nevertheless, applying equations (16) [38] or (20) to model the proposed serial connection of wet links and dry links in the C–S–H gel is clearly wrong. Indeed, in such a case, the relaxation induced by the dissolution-precipitation must be complete. Consequently, in case of serial connection, the strain history $\varepsilon = \mathbb{J}\dot{:}\sigma$ is estimated by trapezoidal approximation:

$$\varepsilon(t_l) = \mathbb{J}(t_l, t_0) : \sigma(t_0) + \sum_{m=0}^{l-1} \frac{1}{2}(\mathbb{J}(t_l, t_m) + \mathbb{J}(t_l, t_{m+1})) : (\sigma(t_{m+1}) - \sigma(t_m)) \tag{21}$$

The integral in equation (14) is discretized by introducing 100 phases representing the drying C-S-H as the cursor c sweeps from $\max_{\tau\in[t,t']}(c_{wet}(RH(\tau)))$ to $\min_{\tau\in[t,t']}(c_{wet}(RH(\tau)))$. It is shown on figure 1.6 that the resulting estimate for the drying creep strain of C-S-H is independent from time discretization and phase discretization. In particular, the phase discretization of the drying C-S-H does not affect the amplitude of drying creep, which is controlled by the parameter β (fig. 1.7).

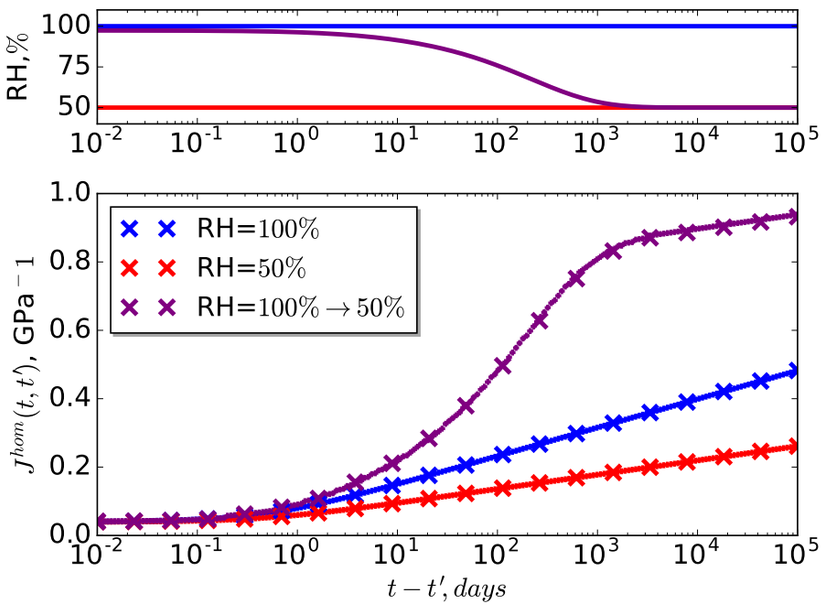

Figure 1.6: The estimated compliance of a C–S–H at C/S ratio of 1.7 is plotted for different evolutions of the relative humidity RH. Either 20 (crosses) or 200 (dots) time steps are considered. While a C–S–H kept at 50%RH creeps less than a C–S–H kept at 100%RH, the drying C–S–H creeps significantly more than the wet C–S–H thanks to the nearly serial connection between dry and wet C–S–H.

2. Comparison to existing experiments and reference results

2.1. Existing estimates of the compliance of the C–S–H gel

Estimates of the compliance of the C–S–H gel have already been produced, either by performing nanoindentation tests [28] or by backward identification [29]. The elastic stiffness of C–S–H is always set according to the indentation results reported in [20], by performing a mix between C–S–H LD and C–S–H HD. A time -independent Poisson ratio is also often set to 0.24 for C–S–H gel, except in [26], where the non-elastic component of the compliance is assumed to be purely deviatoric.

Regarding its uniaxial response, the proposed uniaxial compliance for saturated C–S–H stemming from nanoindentation measurements is consistent with that obtained by backward identification in [26] and [64] (fig. 2.1). Both these models assumes that the Portlandite and AFt phase are purely elastic, as performed in the present study. The compliance reported

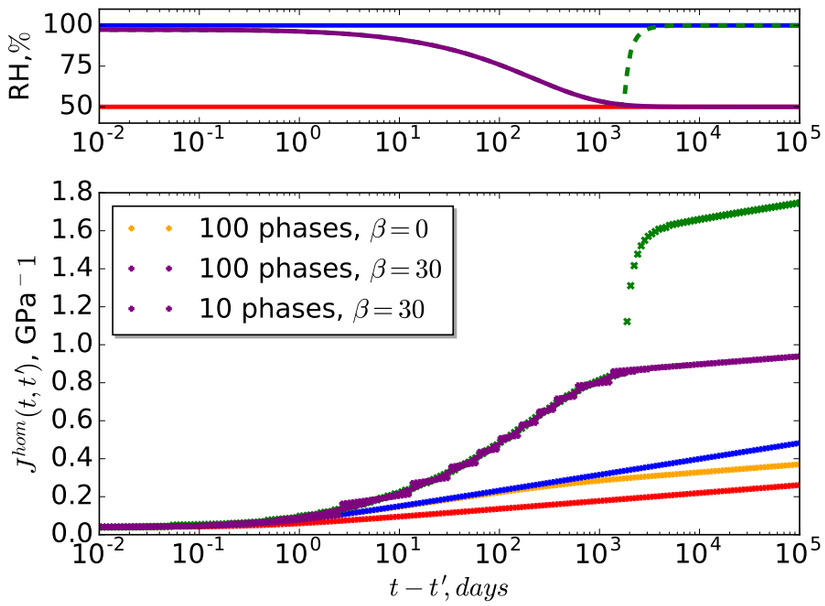

Figure 1.7: The estimated compliance of a C–S–H at C/S ratio of 1.7 is plotted for different evolutions of the relative humidity RH. The number of time step is set to 200. Setting $\beta = 30$ instead of $\beta = 0$ raises the drying creep strains. The number of phases of drying C-S-H is changed for 100 to 10 without affecting the estimated strains (purple curves). Rewetting (green curve) induces an increase of creep strains.

source	compliance type	uniaxial compliance $J(t,t') =$	parameters
[29]	B3 [12]	$q_1 + q_3 \ln(1 + \left(\frac{t-t'}{\tau}\right)^n) + q_4 \ln(\frac{t}{t'})$	$q_1 = 0.0381\text{GPa}^{-1}$, $q_3 = 0.04\text{GPa}^{-1}$, $q_4 = 0.002\text{GPa}^{-1}$, $n = 0.25$, $\tau = 1\text{day}$
[28, 36]	logarithmic	$1/E + 1/E_{\mathbb{D}} \ln(1 + \left(\frac{t-t'}{\tau}\right))$	$E = 25.5\text{GPa}$, $E_{\mathbb{D}} = 1588.9\text{GPa}(\eta - 0.5)^{1.597}(1-\nu^2)$,$\eta = 0.7$, $\tau = 1.66\text{s}$, $\nu = 0.24$
[64]	Kelvin-Voigt	$1/E + 1/E_1(1 - \exp\left(-\frac{t-t'}{\tau_1}\right)) + 1/E_2(1 - \exp\left(-\frac{t-t'}{\tau_2}\right))$	$E = 25.5\text{GPa}$, $E_1 = 12.3\text{GPa}$, $E_2 = 22.5\text{GPa}$, $\tau_1 = 1\text{day}$, $\tau_2 = 10\text{days}$
[26]	logarithmic	$1/E + \frac{1}{3}J^{dev} \ln(1 + \left(\frac{t-t'}{\tau}\right))$	$E = 21.7$–29.4GPa, $J^{dev} \approx 0.175\text{GPa}^{-1}$, $\tau_1 \approx 1\text{hour}$

Table 2.1: Uniaxial compliance of C–S–H as estimated by different studies.

in [28, 36] stems from [8], where the relative humidity during the nanoindentation tests is not reported. Assuming a C/S ratio of 1.7, the logarithmic trend at a packing ratio of $\eta = 0.7$ considered in [28, 36] corresponds to a relative humidity of 24% according to equation (11). In [28], the magnitude of the basic creep tests on cement paste at age 18h, 24h and 30h [65] is correctly recovered because the packing densities at these ages are lower (respectively set to η =0.56, 0.60 and 0.63), thus decreasing the long term moduli to values ($E_{\mathbb{D}}/E = 0.66, 1.5, 2.6$) roughly comparable to that reported for 99% RH-50% RH in the proposed model ($E_{\mathbb{D}}/E = 1.1, 2.2$). Finally, the proposed estimate of the compliance proved largely different from those identified in [29] on 2 and 30 year-old cement paste samples tested at 96% RH [65, 66].

2.2. Microindentation tests on cement pastes

Microindentation tests on numerous CH + C–S–H compacts and C2S / C3S pastes have been performed in [10] at different relative humidities. Since volume fractions of the constitutive phases are also reported, the homogenization procedure can be run without considering the hydration model. As noticed in [10], Eshelby based homogenization schemes are able to provide reasonable estimates for E and $E_{\mathbb{D}}$ as long as the volume fraction of Portlandite is limited ($< 80\%$). The errors on the estimated Young moduli E and logarithmic moduli $E_{\mathbb{D}}$ are plotted on figure 2.2. Since the Portlandite is presently considered as purely elastic, a C3S paste is expected to creep less than a C2S paste featuring the same Young modulus

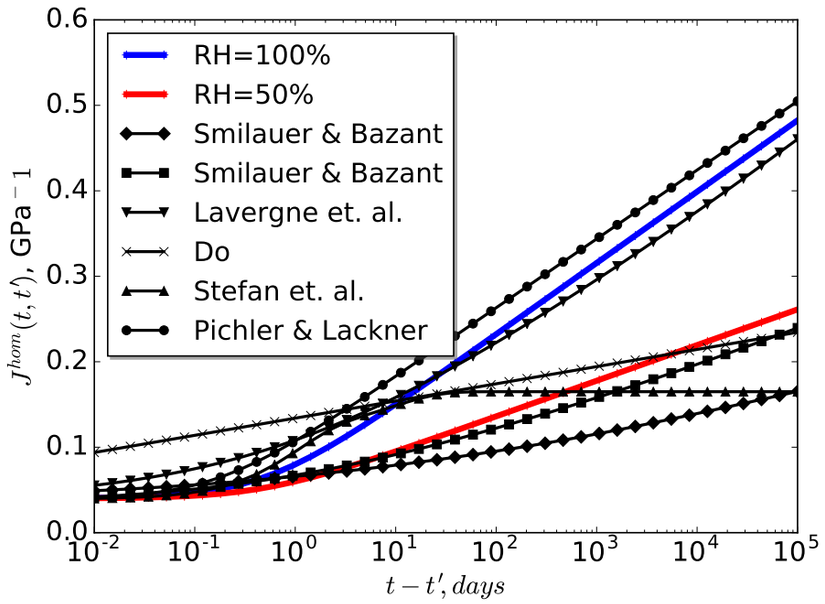

Figure 2.1: The compliance for C-S-H at 100% RH and 50% RH are compared to the compliances for C-S-H reported in the literature by Šmilauer and Bažant [29] from a 30 year old cement paste, Lavergne et al. [33], Do [28], Stefan et al. [64], Pichler and Lackner [26] (tab. 2.1).

as it contains less C-S-H. Furthermore, for C3S paste, the estimated logarithmic modulus $E_{\mathbb{D}}$ varies almost directly with the Young modulus E for different w/c ratios and degrees of hydration. Indeed, modifying the hydration degree or the w/c ratio mainly affect the results of indentation tests by altering the capillary porosity. As explained in section 1.3.1 on page 7, the elastic indentation modulus and the contact creep modulus are likely scaled by the same factor if the volume fraction or morphology of pores is modified. The estimated moduli are globally consistent with the measured moduli, though significant differences are visible.

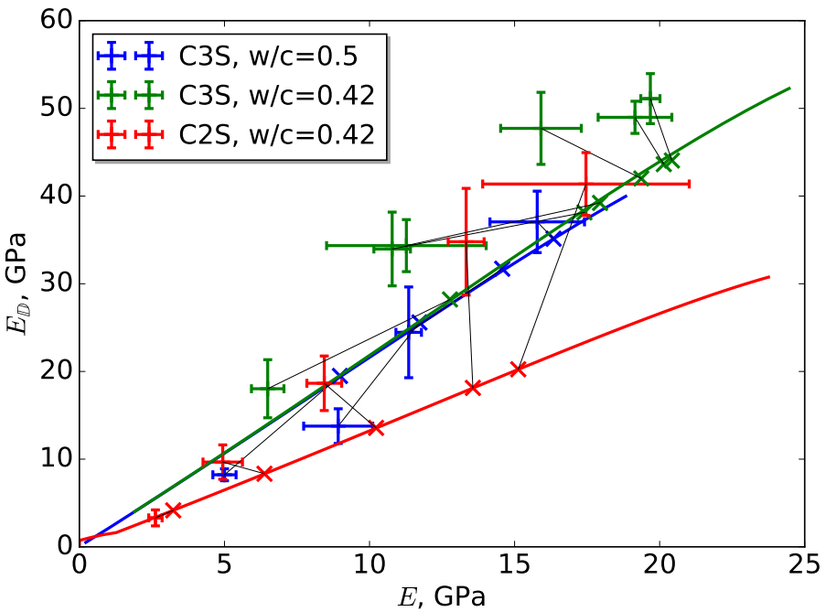

Figure 2.2: The elastic moduli E and the moduli of the logarithmic component $E_{\mathbb{D}}$ are measured by microindentation (errorbars) [10] and estimated by the proposed model (cross). C2S and C3S pastes are tested at different ages in saturated conditions.

2.3. Basic creep tests from the NU database

2.3.1. Modifications suggested to the NU database

Numerous creep tests have been gathered in the NU Database of Laboratory Creep and Shrinkage data so as to evaluate and adjust creep models. The database covers an extended range of strengths, age at loading, environmental conditions and proportions. Hence, the differences between the measured compliances are larger than experimental uncertainties and clear trends can be observed. Nevertheless, there a few metadata of the latest version of the database (CreepShrinkData_20170123GB.xlsx) may be more accurately depicted. For instance, the cement of tests c100_01 – c102_05 and c109_x are classified as RS (Rapid Strength), while the dimensions, environmental conditions and proportions are related to those of the creep tests reported by Hanson [15]. These mass concretes were respectively formulated to build the Canyon Ferry dam, the Shasta dam and the Ross dam, using type II (moderate heat) cement blended with 30% fly ash, type IV (low heat) cement and type II cement. Entries c002_01–_06 and c101_01,c102_01–_05 correspond to the same creep tests and feature similar measured compliances. Their metadata are also similar, but the age at loading of c002_01 must be changed from 28 days to 2 days, to match measured values reported in [15]. In addition, all aggregate to cement ratios could be modified: only small aggregates are accounted for in c002_01 while all aggregates of the mass concrete are accounted for in c101_01. The former is correct, since the aggregates larger than 1-1/2" were screened before casting the 6" diameter cylinders, as reported in [15]. The Japanese JCI database has been integrated in the NU Database by adding sand and coarse aggregate to define the aggregate to cement ratio but only the sand to cement ratio seemed to be considered as the tests of Persson c128_x were incorporated [67]. Furthermore, the elastic strains are likely not included in the compliances reported for tests c_074_x of Brooks [68] though it should be the case according to the metadata. For instance, in the entry c074_23, the compliance at t-t'=1.98 days is valued at 8.74 10^{-6}/MPa, while the secant Young modulus at the time of loading is 29.8GPa. Such a Young modulus would induce a compliance of at least 33 10^{-6}/MPa shortly after loading. Similarly, elastic strains may have been subtracted from compliances of tests J_012_x, J_046_x, D_007_x, D_022_02, D_022_03 and D_040_x. Finally, one of the major entry of the database and creep models is the water to cement ratio. While the majority of tests likely refers to the effective water to cement ratio [16, 69], some others likely refers to the total water to cement ratio [3, 70, 67]. The difference is significant due to the absorption of sand and aggregates [59]. For instance, while the cement ratio of the concrete c_120_01 (Chooz) is reported as 0.543 in the database, its reconstituted cementitious matrix features a water to cement ratio of 0.491 to account for the absorption of water by aggregates [3]. Hence its effective water to cement ratio could be modified to 0.491. The proportioning of the concrete c_123_01 [70] is described in [71], where the w/c ratio of 0.5 refers to total water and it is reported that both fine and coarse aggregates were dried before use. These proposed modifications might improve models relying on this database for the assessment of their accuracy or backward identification of model parameters.

The proposed model is sometimes trustworthy enough for inaccurate metadata to be spotted and corrected according to published references. For each tests, the accuracy of the model is analyzed by mean of statistical indicators [72]. For instance, the coefficient of variation ω_{BP} as defined for the B3 model quantifies the adequacy between observed and estimated values. Let's consider a set of N tests. The overall coefficient ω_{BP} depends on the coefficient ω_i or each test:

$$\omega_{BP} = \sqrt{\frac{1}{N}\sum_{i=1}^{N}\omega_i^2} \tag{22}$$

The coefficient of variation of a test depends on the difference between observed and estimated compliance $J_{i,exp}(\delta t_j)$ and $J_{i,mod}(\delta t_j)$:

$$\omega_i = \frac{1}{J_i}\sqrt{\frac{1}{n-1}\sum_{j=1}^{n} w_{ij}(J_{i,mod}(\delta t_j) - J_{i,exp}(\delta t_j))^2} \tag{23}$$

where n is the number of points in the test i and $w_{ij} = n/(n_d n_j)$ is a weight balancing the importance of each decade in the measurement of the error. Indeed, n_d is the number of decades covered by the test and n_j is the number of points in the same decade as δt_j, where decades are $\delta t < 10$ days, $10 \leq \delta t < 100$ days, $100 \leq \delta t < 1000$ days and $\delta t \geq 1000$ days. The weight $1/J_i$ balances tests featuring small or big compliances and it make the coefficient

of variation unitless.

$$J_i = \frac{\sum_{j=1}^{n} w_{ij} J_{i,exp}(\delta t_j)}{\sum_{j=1}^{n} w_{ij}} \tag{24}$$

Finally, ω_{BP} can be viewed as an estimate of the coefficient of variation of the relative error of the model, where weights have been carefully defined for each point so as to reduce the sensitivity to time steps δt_j, to the magnitude of the compliance J_i or to the number of points n in test i:

$$\omega_{BP} = \sqrt{\sum_{i=1}^{N} \sum_{j=1}^{n} \frac{1}{N} \frac{1}{n-1} \left(\frac{J_{i,exp}(\delta t_j)}{J_i} \right)^2 w_{ij} \left(\frac{J_{i,mod}(\delta t_j) - J_{i,exp}(\delta t_j)}{J_{i,exp}(\delta t_j)} \right)^2} \tag{25}$$

In addition, the CEB mean deviations M_{CEB} computed for range of time elapsed since loading describes whether the model underestimates or overestimates the time dependent strains [72]. For a given test i, M_{CEB} is defined as an average of deviations M_{ik} computed on 6 time ranges: $\delta t < 10$ days, $10 \leq \delta t < 100$ days, $100 \leq \delta t < 365$, $365 \leq \delta t < 730$ days, $730 \leq \delta t < 1095$ and $\delta t \geq 1095$ days. On a given time range k, it writes:

$$M_{ik} = \frac{1}{n_k} \sum_{j=1}^{n_k} \frac{J_{i,mod}(\delta t_j)}{J_{i,exp}(\delta t_j)} \tag{26}$$

where n_k is the number of point of test i in the time range k.

The outcome of a first run of the model for basic creep tests including the elastic strains is interesting as some tests feature big coefficients of variation. On the one hand, the model may significantly overestimate the time-dependent strains. Most of these tests refer to concretes loaded at early age, before 3 days. Indeed, such situations require a refined estimate of the maturity of concrete and the homogenization schemes are challenged by high capillary porosities. On the other hand, the time dependent strain can be underestimated. For instance, while the creep strains of tests c_051_01, c_051_03, c_051_09, c_051_11 are correctly estimated, those of tests c_051_15 are underestimated. The discrepancy is to be attributed to the aggregate type. Indeed, the low modulus aggregate (Graywacke) of test c_051_15 is particularly soft ($E = 26$ GPa, $\nu = 0.15$), while the other aggregates (Chert and Limestone) are stiffer (respectively $E = 94$ GPa, $\nu = 0.13$ and $E = 72$ GPa, $\nu = 0.3$) [16]. Similarly, the creep strains of the tests c_015_01 and c_015_05 loaded at 8 days are underestimated though the cement is correctly reported to be a type III cement [73]. Indeed, the instantaneous compliance is reported to be 47.6 10^{-6}/MPa, corresponding to a Young modulus of 21 GPa. This Young modulus is surprisingly low, given the w/c ratio of 0.46 of that concrete. More specifically, the Young modulus at 14 days was measured at 23 GPa and the compressive strength at 43 MPa, the density being 2.36 t/m^3 [73]: according to Eurocode 2 (quartzite) and ACI standards, the Young modulus would have being expected to be 34 GPa and 31 GPa. The error could be reduced by assuming the Santa Clara river aggregates to be softer or less adhesive: occurrence of sandstone and granitic rocks have been reported [74]. The basic creep of concretes c_025_x, c_032_x and c_110_01, c_110_02 loaded at at 20°C is also underestimated. The ordinary Portland cement considered by Browne [75, 76, 77] for these tests was considered to build pressure vessels more than 3 meters thick and such structures were built using type II moderate heat cement [78]. Therefore, by assuming the cement to be normal or rapid, its hydration degree may be overestimated by the model, thus partly explaining the error. The same reasoning applies to the creep strains of tests c_112_x and c_113_x. Indeed, the database does not report the cement type, but a moderate heat type II cement was blended with calcined shale to formulate this concrete dedicated to the Dworshak dam [15]. Hence, the model underestimates the creep strains, as it assumes the binder to be pure normal or rapid cement. The model also underestimates the creep strains of tests c_072_02, c_072_04 and c_072_05 at all times: the hydration degree and the estimated mechanical responses of concrete samples featuring a slump of about 50mm, w/c ratios in the range 0.27–0.3 but stored in water for 28 days is likely inaccurate. Creep strains of tests J_018_1–13 on concretes formulated for the Kurobe 4 and Tonoyama arch dams featuring slumps in the range 30–35mm and made of moderate heat Portland cements are also underestimated at all times. The concrete of tests J_022_08+ also induces underestimated basic creep strains at all time elapsed since loading: its binder includes an expansive admixture based on CSA cement (13%wt) and the w/c ratio is 0.44. This admixture might compete against Portland cement for water and form other hydration products, thus affecting the mechanical properties.

While the tests of Maia et. al. [79] D_029_x are depicted as basic creep tests in the database, these samples were unmolded at 23h, stored at 50% RH and loaded at 3 or 7 days

reference	modifications
c_002_01	$t' = 2$ days
c100_x	$w/c = 0.71$, $a/c = 12.$, $c = 168\text{kg/m}^3$, cem=SL, cem_prov=type II, FlyAsh/c=42%wt
c101_x	$w/c = 0.58$, $a/c = 5.62$, $c = 346\text{kg/m}^3$, cem=SL, cem_prov=type IV
c102_x, c109_x	$w/c = 0.56$, $a/c = 6.14$, $c = 320\text{kg/m}^3$, cem=SL, cem_prov=type II
c128_x	$a/c = \{4; 4.06; 3.82; 4.12; 3.56; 3.28; 3.7; 3.22\}$
c074_x	Add elastic strains, moduli reported in [68]
J_012_x	Add elastic strains (0–10):E=35.672GPa , (11–22):E=36.358GPa $f_c = 41.7$MPa
J_046_x	elastic strain=no
D_007_x	Add metakaolin as silica fume, add elastic strains, moduli reported in [103]
D_022_02–03	elastic strain=no
D_040_x	elastic strain=no
D_024_x	remove values flagged for deletion and compliance lower than 20e-6/MPa
D_029_x	type=drying [79]
D_045_2-3-5-7	type=drying [80]
c_120_01–06	$w/c = \{0.491; 0.459; 0.438; 0.438; 0.489; 0.541\}$. a/c, silica fume and filler also corrected. fc_{28} reordered, E_{28} corrected [3].
c_123_01	w/c modified by assuming absorption of sand and gravel of 1% and 0.5%
c_051_15	Graywacke (E=26 GPa, ν =0.15)
c_025_x, c_032_x, c_110_x	cem=SL, cem_prov=type II
c_112_x, c_113_x	$w/c = 0.8$, $a/c = 9.7$, $c = 195\text{kg/m}^3$, cem=SL, cem_prov=type II, FlyAsh/c=35%
c_017_x	$w/c = 0.45$, cem=N, 20% slag.
c_074_x	cem=RS

Table 2.2: Modifications operated on the NU Database.

: the dimensions of the samples are such that drying is likely occurring during the creep test. The tests D_045_2-3-5-7 are drying creep tests too [80]. Finally, the tensile creep tests J_047_03 and J_047_02 feature both an overestimated elastic compliance and underestimated creep strains: the tensile stresses of -1.2MPa and -1.6 MPa are likely out of the linearity range of basic creep, since the comparison to the test J_047_01 at a lower tensile stress of -0.8 MPa on the same concrete exhibits a lower coefficient of variation. As a consequence, most of extreme discrepancies between estimated creep strains and measured creep strains proved related to missing details about the formulation or tests conditions: it unveils the reliability of the model.

In the course of the bibliographic review of the sources of the database, some additional details are to be signalled. For instance, the cement used for the longest available creep tests, loaded at 14 days, is a rapid-hardening Portland cement [81]. While North Notts aggregates are reported to be a good aggregate, those of Stourton are described as poor quality rounded aggregates. The density of the North Notts, Strouton, Aglite and Lytag coarse aggregates are modified according to the cement paste volume fraction reported in [81]. The binder and proportions of tests c_017_x also needs a refined description. Indeed, deemed CPB 250/315, of density 3.04, it is a Portland cement blended with about 20% slag, of Blaine fineness $315\text{m}^2/\text{kg}$ [82]. Its oxide composition (SiO_2=23.35%, Fe_2O_3=2.25%, Al_2O_3=7.35%, CaO=59.2%, MgO=1.45%, SO_3=2.%) clearly differs from that of a pure Portland cement. Nevertheless, this binder enters the 42.5N class: the compressive strength of the normal mortar reaches 13.2MPa at 2 days, 29.4MPa at 7 days and 43.4MPa at 28 days. This binder hardly fits into classes considered in creep models and could enter the CEB class 'N', but it likely gains significant strength after 28 days. In the present model, the slag is roughly considered as belite, as a precise modelling of slag hydration is not implemented yet. The w/c ratio of 0.49 also refers to the dry mix [82]: the effective w/c ratio is likely closer to 0.45 once assumed absorptions of sand and gravel of 1% and 0.5% are accounted for. Lastly, the w/c ratio of the Ultra High Performance Concrete investigated in [83] is likely lower than 0.5: the article reports that the volume fraction of cement paste is 50%, but the w/c ratio and proportions of the mix are not thoroughly described. Corresponding tests are therefore discarded from the comparison. Finally, suggested modifications to the NU database are reported in table 2.2 and additional metadata accounted for are reported in table 2.3. These modifications are operated for the final comparisons performed in the next section.

2.3.2. Outcome of the comparison to the modified database

The comparison between the estimated compliances and those measured can be plotted for particular datasets (fig. 2.3) and the corresponding statistical indicators are reported in table 2.4 for 311 basic creep tests loaded after 3 days, stored at room temperature, for which the elastic strain has been measured. The creep strain is said to be overestimated if the CEB mean deviation M_{CEB} exceeds 1.25 or underestimated if it proves lower than 0.75. If all the

reference	modifications	motive
c_017	C3S:47,C2S:34, C3A:2.3, C4AF:10, CSb:3.6, CCb:0.0, Blaine: 315m^2/kg	slag, [82]
c_128	C3S:57,C2S:20.6, C3A:0.82, C4AF:14.5, CSb:3.4, CCb:1.4, Blaine: 302m^2/kg	low C3A, [67]
c_123_01..44	C3S:57,'C2S':17, 'C3A':2.8, 'C4AF':12., CSb:4.3, CCb:3.4, Blaine: 365m^2/kg	Saint Vigor [70]
c_123_45..47	C3S:60,C2S:12, C3A:8.6, C4AF:8.2, 'CSb:5.7, CCb:3.0, Blaine: 410m^2/kg	Saint Pierre la Cour [70]
c_051_01..08	$\rho_a = 2.52$, $E_a = 93$GPa, $\nu_a = 0.12$	chert, [16]
c_051_09..14	$\rho_a = 2.7$, $E_a = 69$GPa, $\nu_a = 0.3$	limestone, [16]
c_051_15..19	$\rho_a = 2.7$, $E_a = 28$GPa, $\nu_a = 0.15$	graywacke, [16]
c_074_..	$sand/a = 1.71/4.75$, $ca/a = 3.04/4.75$, $\rho_{ca} = 2.7$, $E_{ca} = 70$GPa, $\nu_{ca} = 0.1$	North Notts. [81]
c_074_..	$sand/a = 1.71/4.75$, $ca/a = 3.04/4.75$, $\rho_{ca} = 2.55$, $E_{ca} = 25$GPa, $\nu_{ca} = 0.1$	Stourton [81]
c_074_..	$sand/a = 1.71/4.75$, $ca/a = 1.52/4.75$, $\rho_{ca} = 1.4$, $E_{ca} = 15$GPa, $\nu_{ca} = 0.15$	Aglite [81]
c_074_..	$sand/a = 1.71/4.75$, $ca/a = 1.52/4.75$, $\rho_{ca} = 1.8$, $E_{ca} = 25$GPa, $\nu_{ca} = 0.15$	Lytag [81]

Table 2.3: Additional metadata provided to the hydration model and micro-mechanical scheme.

tests loaded after 3 days are considered, the overall coefficient of variation $w_{BP} = 0.32$ is rather high (tab. 2.4).

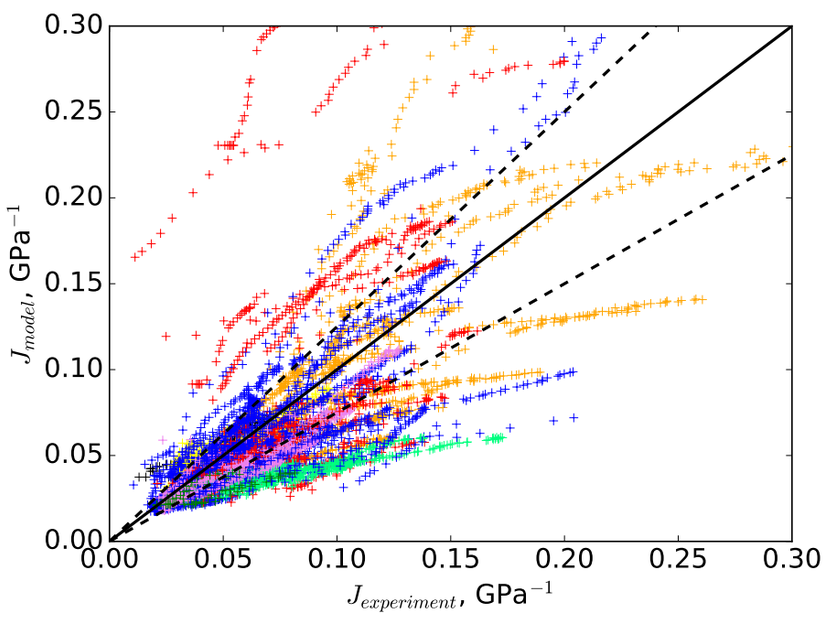

Figure 2.3: The estimated compliance is compared to that measured. Red: samples loaded before 3 days. Orange: tests c_074 of Brooks [68]. Spring green: tests on concrete featuring a low slump J_003 and J_018. Violet: tests J_012, D_024, D_022, D_007, elastic strains being accounted for.

The proposed model can be updated on the base of short-time tests, as proposed for existing models. It is hereby proposed to revise the estimated time-dependent strains by accounting for the measured Young modulus at time of loading or the first valuable measure of the strain after loading. The procedure simply consists in scaling the estimated time-dependent strains so that the estimated instantaneous strains becomes consistent with that measured: it corresponds to keeping the estimated $\Phi(t,t') = J(t,t')E(t') - 1$ function unaltered. A theoretical foundation can be proposed following the reasoning presented in section 1.3.1, on page 7: scaling the time-dependent strains is equivalent to attributing the error to the porosity not being properly accounted for. Indeed, adding porosity or modifying the morphology of a porous network only results in a scaling of the time-dependent strains, as long as the solid skeleton is assumed to be linear viscoelastic, uniform in time and space

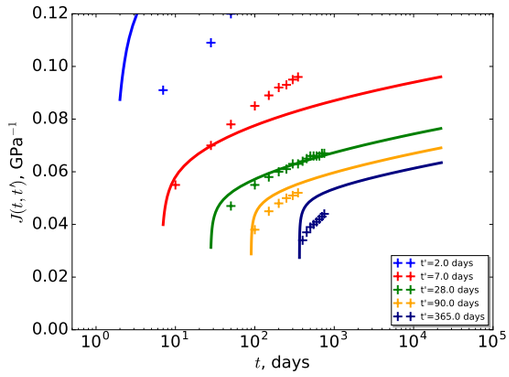

(a) Hanson, $w/c = 0.56$, $a/c = 6.14$, $c = 320$ [15]

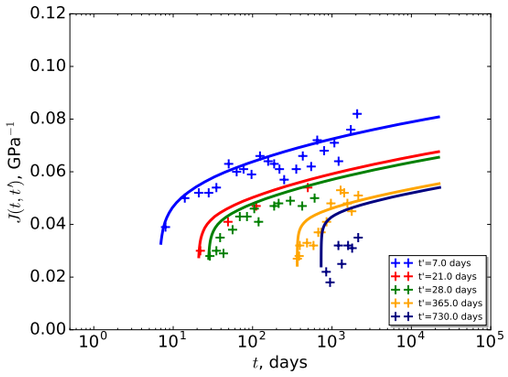

(b) L'Hermite et Mamillan, $w/b = 0.45$, $a/b = 4.81$, $b = 350$, cement+slag [82]

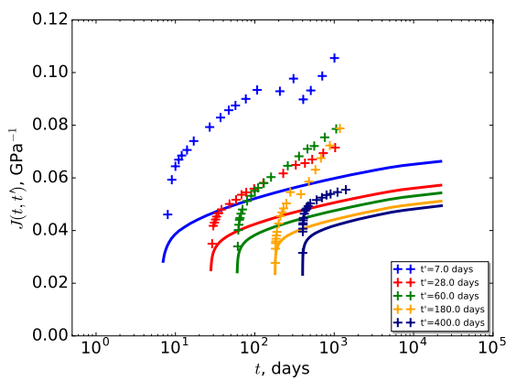

(c) Browne, $w/c = 0.42$, $a/c = 4.40$, $c = 418$ [75, 76, 77]

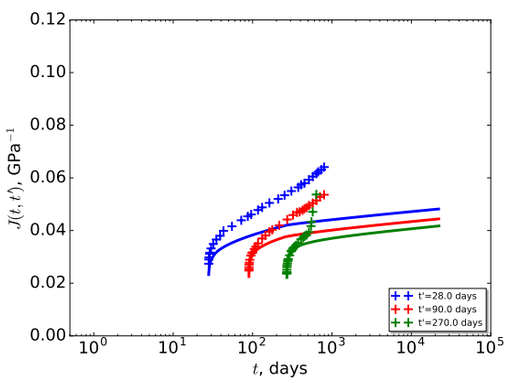

(d) Kommendant, $w/c = 0.38$, $a/c = 4.34$, $c = 419$

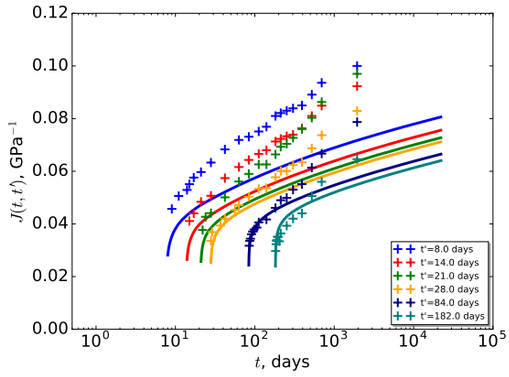

(e) Shritharan, $w/c = 0.47$, $a/c = 5.09$, $c = 390$

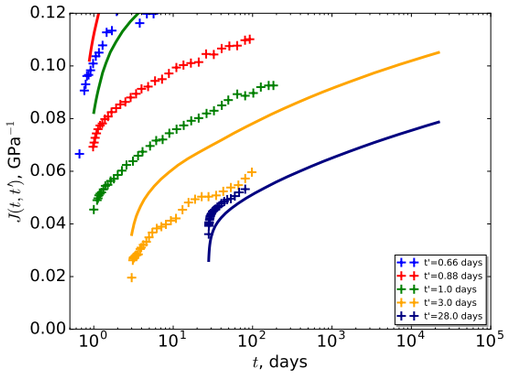

(f) Anders, $w/c = 0.45$, $a/c = 3.93$, $c = 435$

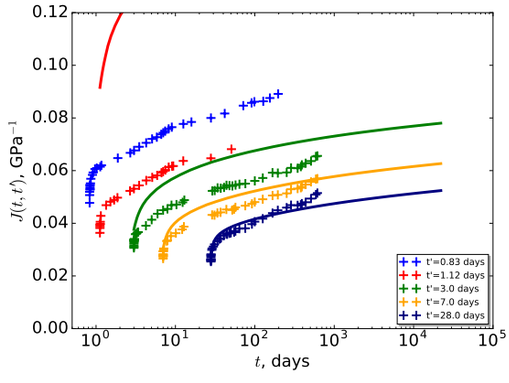

(g) Le Roy, $w/c = 0.463$, $a/c = 5.46$, $c = 342$ [71, 70]

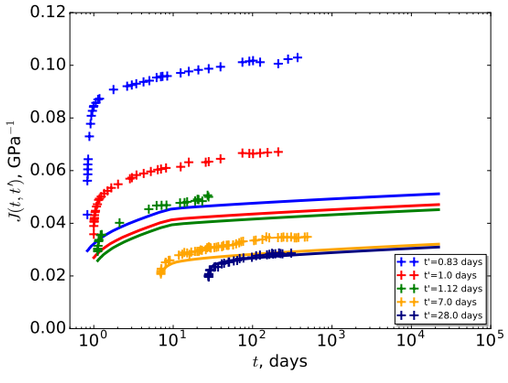

(h) Le Roy, $w/c = 0.298$, $a/c = 4.73$, $c = 398$, +10% silica fume [71, 70]

and features a time-independent Poisson ratio. This is clearly a plausible explanation for the error on the estimated time-dependent strains induced by particular features of the concrete. For instance, the inaccuracy on the porosity could stem from the air entrainment or the

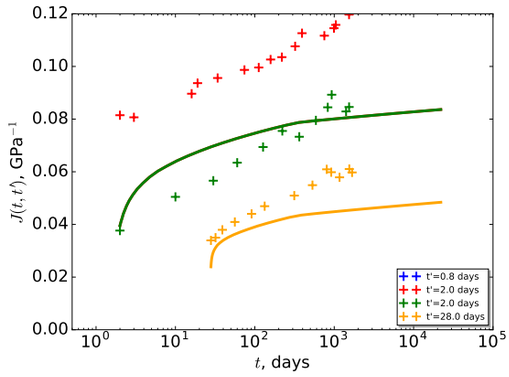

(i) Persson, $w/c = 0.38$, $a/c = 4.$, $c = 430$, +4.9% silica fume [67]

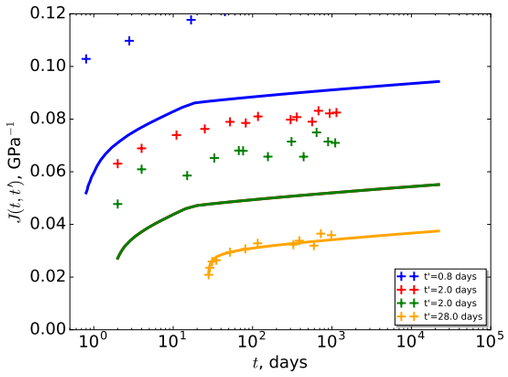

(j) Persson, $w/c = 0.3$, $a/c = 3.28$, $c = 530$, +9.6% silica fume [67]

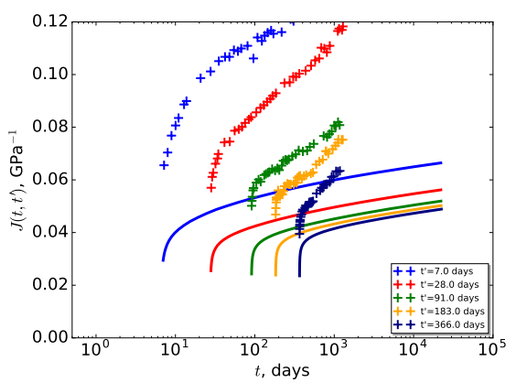

(k) Kawasumi, $w/c = 0.47$, $a/c = 6.01$, $c = 304$

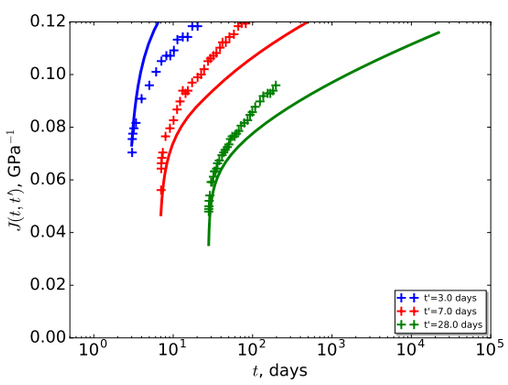

(l) Ohnuma, $w/c = 0.63$, $a/c = 5.75$, $c = 299$

Figure 2.4: The estimated basic creep strains (lines) are compared to those measured (plus signs) for some studies having performed loading at different ages.

compaction process for concretes featuring a low slump. Mis-estimating the final hydration degree of low w/c concretes mainly affects the estimated strains through the incorrect capillary porosity. Finally, an error on the effective w/c ratio, a porosity softening the aggregates, imperfect bonding between the paste and the aggregates, a non-evolving micro-cracking in the paste, or an evenly distributed capillary porosity induced by an interfacial transition zone can be roughly described as modifications of the pore network and would therefore globally induce a scaling of both instantaneous and time-dependent strains by the same factor.

The result of the scaling is displayed on figures 2.5 and 2.6: there are a few points featuring an absolute relative error on the time-dependent strains higher than 25% compared to the uncorrected estimate 2.3. These points are mostly related to concretes loaded before three days, tensile creep tests or to the long-term tests of Brooks [68]. All points featuring an underestimated creep strain lower than 60% of the measured strain belong to 7 tests out of 311: a test on an concrete featuring w/c ratios higher than 0.6 loaded at 3 days (D_024_14), the tests c_074_19 and c_113_05 (w/c=0.8), tests on a concrete of w/c=0.45 loaded at 730 days featuring a measured Young modulus of 60GPa (c_017_21 and c_017_25) and tensile creep tests (J_047_02 and J_047_03). For concrete loaded at early age, the error is mostly due to the mis-estimated maturity: its effect on the time-dependent strain is not limited to a change of a time-independent porous network and scaling does not efficiently correct it. As a consequence, tuning the properties of the cement so as to match the observed Young modulus at the time of loading might prove more efficient. Regarding the tests of Brooks, it is to be recalled that the samples were stored in water for decades, thus prompting extra hydration or a lixiviation as potential origins for the observed important creep strains. Scaling also globally reduces the mismatch between the estimates and the measurements as quantified by the statistic indicators (tab. 2.4). Furthermore, if the comparison is limited to the 202 compressive tests featuring a w/c ratio lower than 0.55 and loaded after 7 days, the w_{BP} is down to 0.15 after scaling and the measured strain is likely lower than $\gamma = 1.32$ times the scaled estimated strain (95% probability) (Fig. 2.6). This factor could be adopted so as to avoid underestimating the prestress losses induced by the basic creep of concrete. Lastly, the correction proves particularly effective for concretes featuring a small slump: the scaling stems

as the most effective way to account for the porosity induced by the air entraining agents and the compaction process. This correction requires a measurement of a Young modulus of the concrete at the time of loading, a piece of information that is not always available as the structure is designed. Nevertheless, the coefficient of variation of the unscaled estimate of basic creep remains important ($w_{BP} = 0.29$) even if the comparison is limited to these 202 tests. To the author's opinion, a requirement on the Young modulus at the time of loading seems essential for designing sensitive pre-stressed structures and a creep test lasting a few months clearly remains of valuable interest.

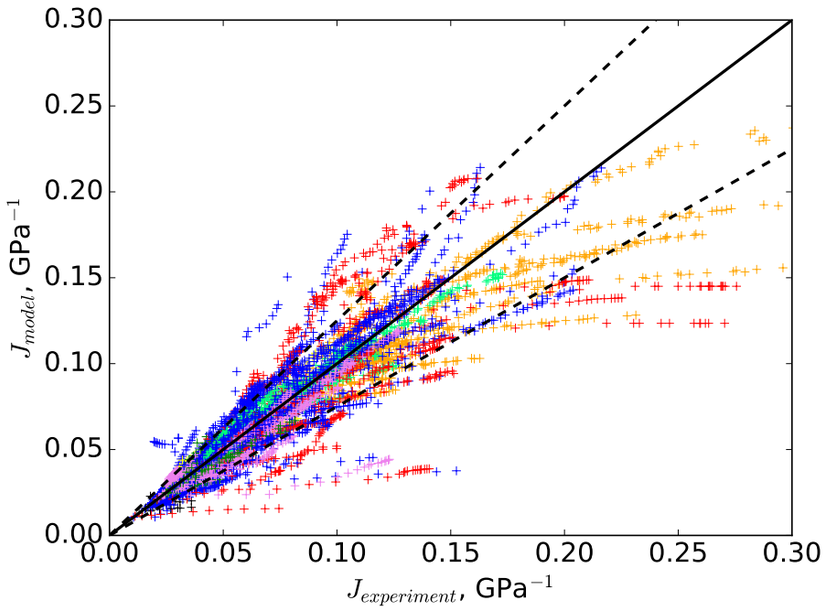

Figure 2.5: The estimated compliance after accounting for the Young modulus by scaling is compared to that measured. Red: samples loaded before 3 days. Orange: tests c_074 of Brooks [68]. Spring green: tests on concrete featuring a low slump J_003 and J_018. Violet: tests J_012, D_024, D_022, D_007, elastic strains being accounted for.

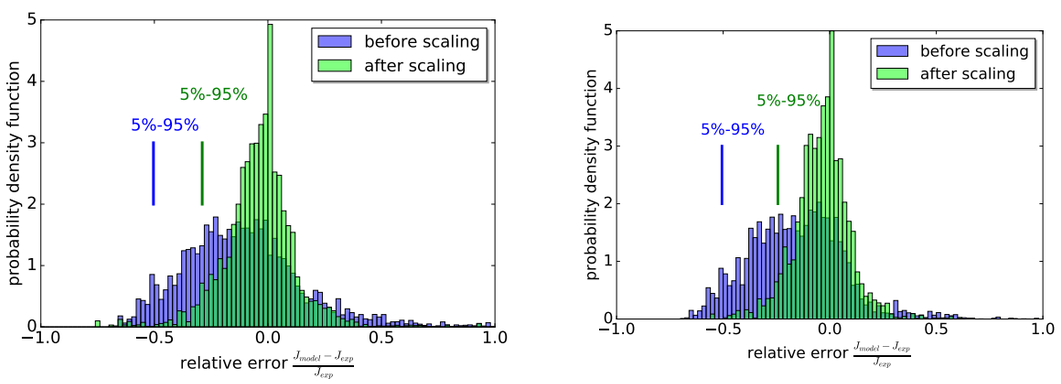

Figure 2.6: Left: the distributions of the relative error of the unscaled and scaled estimated of the basic creep compliance are plotted for 319 creep tests. Points are weighted as implicitly defined by the w_{BP} statistical indicator. Scaling clearly improve the estimate. Right: the distributions are plotted for 202 compressive creep tests on concrete featuring w/c ratios lower than 0.55 and loaded after 7 days.

The proposed model is compared to existing models, such as ACI209-R92 [72], CEB90-99 ($\approx$ Eurocode 2 1-1) [84], B3 [12], AFREM ($\approx$ Eurocode 2 2) [70, 85], GL2000 [86], *fib* MC2010 [14], and B4 [13, 87]. The implementations of these models are checked by reproducing the outputs reported in references [72, 87]. The coefficients of variation are computed for the 311 basic creep tests loaded after 3 days at room temperature before and after scaling (tab. 2.5). While ACI209-R92, CEB90-99 (Eurocode 2 1-1) and AFREM (Eurocode 2 2) do not exhibit abnormal coefficient of variation, these models clearly tend to underestimate the creep strains. Indeed, their bounded compliances lead to underestimated long-term creep strains. On the contrary, models B3, GL2000, B4, *fib* MC2010 and the proposed model have

author	number of tests	ω_{BP}	ω_{BP} updated	comments
Anders	4	0.26+	0.17	[104]
Aoyagi et al.	2	0.32	0.32+	[105]
Arthanari	1	0.59+	0.05	[106]
Aschl & Stöckl	1	0.50+	0.47+	[107]
Brooks	27	0.34+/-	0.18	[81]
Browne	11	0.38-	0.21-	[75, 76, 77]
Dilger	5	0.36-	0.18-	[108]
Dutron	2	0.24	0.05	[109]
Hannant	3	0.29 +	0.07	[110]
Hanson (Hansen in database)	16	0.48 +	0.16	[15]
Hanson	4	0.16	0.10	[15]
Johansen & Best	4	0.19	0.18	[111]
Kanazu et al.	2	0.29 +	0.27 +	tensile creep tests, neither cylindrical nor prismatic samples. [112]
Kawasumi	17	0.47 -	0.09	low slump, moderate heat cement [113]
Keeton	2	0.46 -	0.08	low Young modulus [73]
Kommendant et al.	13	0.15	0.09	[114]
Kumono et al.	3	0.44	0.6 -	tensile creep tests [115]
L'Hermite & Mamillan	17	0.36 +	0.18 -	[82]
de Larrard	2	0.10	0.13	[116]
Le Roy & Laplante	33	0.15 -	0.12 -	[71, 70]
Lee et al.	24	0.28 -	0.21 -	[117]
McDonald	6	0.08	0.10	[16]
Min et al.	4	0.47 -	0.19	[118]
Mossiossian & Gamble	1	0.40 -	0.15	[119]
Navratil	2	0.33 -	0.25	[120]
Ngab et al.	3	0.35 -	0.12	[121]
Ohnuma et al.	28	0.36 +/-	0.15 +	expansive admixture, CSA cement [122, 123]
Okada et al.	4	0.09	0.09	[124]
Okajima et al.	1	0.13	0.12	[125]
Persson	8	0.29 -	0.16	[67, 80]
Pirtz (Dworshak Dam)	8	0.51 +	0.41 +/-	cement type II, calcinated shale [126]
Rostasy et al.	1	0.20	0.10	[127]
Russel & Burg	2	0.18	0.22	[128]
Schwesinger et al.	1	0.18	0.37 +	[129]
Seki & Kawasumi	2	0.28 -	0.04	[130]
Shritharan	6	0.24	0.13	[131]
Takahashi & Kawaguchi	3	0.07	0.13	[132, 133]
Theiner et al.	2	0.35 -	0.05	[134]
Troxel et al.	3	0.20	0.10	[135]
York et al.	4	0.06	0.09	[69]
c_091	25	0.25 +/-	0.13	
all	311	0.32	0.18	
compressive, $w/c < 0.55$, $t_0 \geq$7 days	202	0.29	0.15	

Table 2.4: Statistical indexes gathered by authors are computed for both results accounting for the composition of the concrete and results updated by accounting for the Young moduli. Plus signs and minus signs respectively signal that at least one test features overestimated or underestimated creep strains.

model	number of test	ω_{BP}	ω_{BP} updated
ACI209-R92	311	0.37	0.26
CEB90-99 (Eurocode 2-1)	311	0.31	0.21
B3	311	0.35	0.24
B3, without [70]	311-33	0.28	0.22
AFREM (Eurocode 2-2)	311	0.34	0.22
B4	311	0.45	0.23
fib MC2010	311	0.29	0.18
present model	311	0.32	0.18

Table 2.5: The w_{BP} statistical indicator is computed for each model, for the 311 basic creep tests at room temperature loaded after 3 days. Updating the estimated strain by scaling always significantly improves the accuracy of the model, for all the considered models.

been designed so as to avoid such a bias by making use of a logarithmic long-term trend and should be considered as more reliable. While models B3 and B4 have been adjusted to minimize a w_{BP} indicator, the computed indicator are not lower than indicators of other models. While the B3 model has been adjusted on the smaller RILEM database, it still proves accurate. Indeed, if the 33 tests on high performance concrete from [70] recently added are omitted, w_{BP} of the B3 model is down to 0.28. The w_{BP} indicator of models B3 and B4 compared to the unmodified database are respectively 0.37 and 0.5: using the modified metadata therefore reduces the w_{BP} indicator. It unveils the robustness of these models and leaves room for further improvements. In addition, model B4 has also been adjusted to retrieve the magnitude of measured excessive deflections of prestressed bridges. This is likely the reason why the creep strains predicted by this model may be overestimated when compared to laboratory measurements as presently performed. Finally, for all these models, scaling efficiently reduces the difference between the estimated creep strains and those measured.

2.4. Discussion

2.4.1. Creep recovery tests

The logarithmic compliance $\mathbb{J}$ introduced for the C-S-H at uniform relative humidity in equation (10) is non-aging and entirely recoverable:

$$\lim_{t\to\infty} \mathbb{J}(t,t_1) - \mathbb{J}(t,t_2) = \mathbb{0} \qquad \forall t_1, t_2 \tag{27}$$

As a consequence, the basic creep of a fully hydrated concrete at uniform internal relative humidity is expected to be recoverable. Nevertheless, hydration reactions and change of internal relative humidity induce irrecoverable creep strains related to the dissolution of load-bearing phases and precipitation of stiff phases loaded at unloading.

Furthermore, if a concrete is loaded at early age and unloaded at later age, the unloading might induce tensile stresses in some of the hydrate formed between loading and unloading. Indeed, it is assumed that the new hydrates are free of stress as they precipitate: these new hydrates are only compressed due to changes of the macroscopic strain occurring after their precipitation. The assumption of new hydrates being in equilibrium with the fluid upon precipitation is rooted in the parallel coupling of the solidification theory [5]. It was already noticed in [5] that solidification in stressed state is possible, though it requires a different geometry or the introduction of a crystal growth pressure. Nevertheless, such a crystal growth pressure is unlikely at the scale of the hydrate foam, where plenty of capillary pore space is available and where the degree of supersaturation of ettringite is likely limited [88]. On the contrary, the proposed serial connection between wet C-S-H and dry C-S-H induce a stress in the newly-formed C-S-H right after its formation. Therefore, it might be depicted as a phase equilibrium between solids [89].

2.4.2. The creep Poisson ratio of concrete

Mean field schemes and numerical methods [90] produce estimates of the whole compliance tensor, including the creep Poisson ratio. It is defined as the opposite of the ratio of lateral strain to longitudinal strain during an uniaxial creep test [91] and it affects prestress losses in case of multi-axial prestressing [92]. Other things being equal, the Poisson ratio of the normal aggregate is expected to affect the creep Poisson ratio of the concrete (fig. 2.8). Indeed, the smaller the static Poisson ratio of the aggregate is, the smaller the creep Poisson ratio of the concrete is. Nevertheless, as time elapsed since loading increases, its dependency to the nature

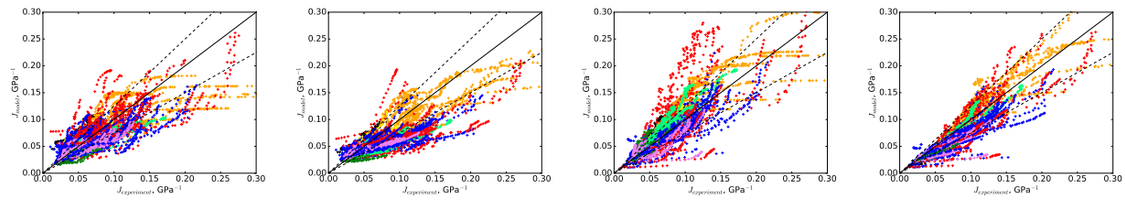

(a) ACI209-R92 (b) CEB90-99 (≈ Eurocode 2-1) (c) ACI209-R92, scaled (d) CEB90-99 (≈ Eurocode 2-1), scaled

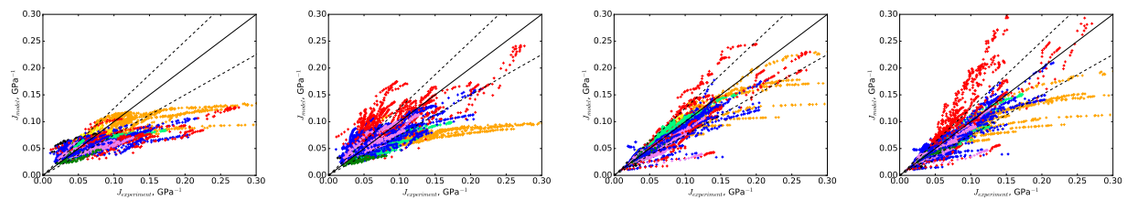

(e) AFREM (≈ Eurocode 2-2) (f) GL2000 (g) AFREM (≈ Eurocode 2-2), scaled (h) GL2000, scaled

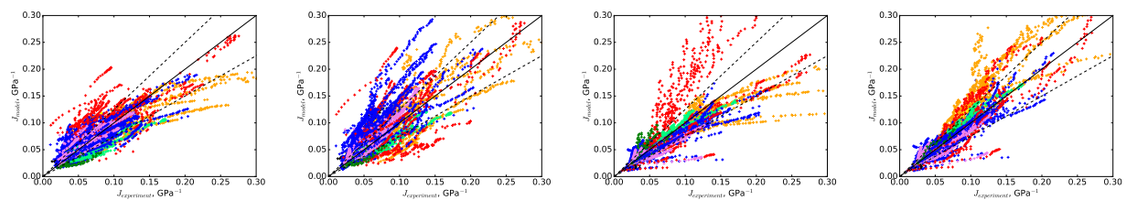

(i) B3 (j) B4 (k) B3, scaled (l) B4, scaled

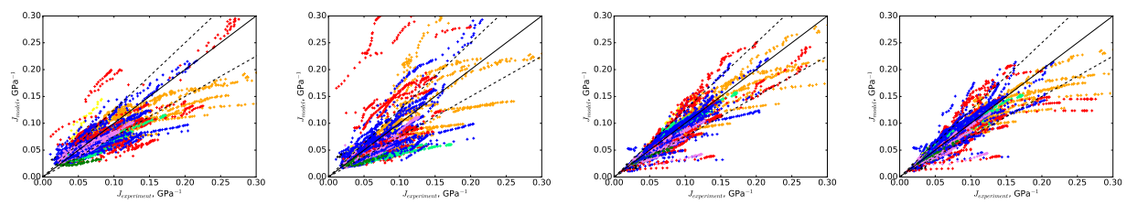

(m) *fib* MC2010 (n) proposed (o) *fib* MC2010, scaled (p) proposed, scaled

Figure 2.7: The estimated compliance is compared to that measured for different creep models. The error is reduced by scaling the estimated strain so as to match the measured Young modulus. Red: samples loaded before 3 days. Orange: tests c_074 of Brooks [68]. Spring green: tests on concrete featuring a low slump J_003 and J_018. Violet: tests J_012, D_024, D_022, D_007, elastic strains being accounted for.

of the aggregate is reduced. Indeed, the strain concentrates in the soft viscous cementitious matrix, thus reducing the share of the aggregates in the average strain. Therefore, the lower the apparent stiffness contrast between the soft cementitious matrix and the stiff aggregate is, the more important the Poisson ratio of the aggregate becomes. As a consequence, the creep Poisson ratio may increase or decrease with the time elapsed since loading, depending on the Poisson ratio of the aggregate. As the creep Poisson ratio of the cementitious matrix is also slightly time-depend, that of the concrete might be non-monotonous. In addition, the lateral creep strains of high performance concretes (stiff matrix) and lightweight concretes (soft aggregates) are likely more sensitive to the Poisson ratio of the aggregate. Finally, the estimated evolution of the creep Poisson ratio remains moderate, which is consistent with the assumption of a time-independent Poisson ratio for all phases performed in the model. Most of existing models of the time dependent strains of concretes assume that the creep Poisson ratio of concrete is time-independent.

2.4.3. Limits of the proposed model

Given the results of the comparison to the NU database, the following limits can be suggested.

- The proposed model is too inaccurate to produce valuable estimates of the basic creep strains if the concrete is loaded before 3 days, as long as the cement is only described by its type. Providing the Bogue composition and the Blaine fineness could partly resolve

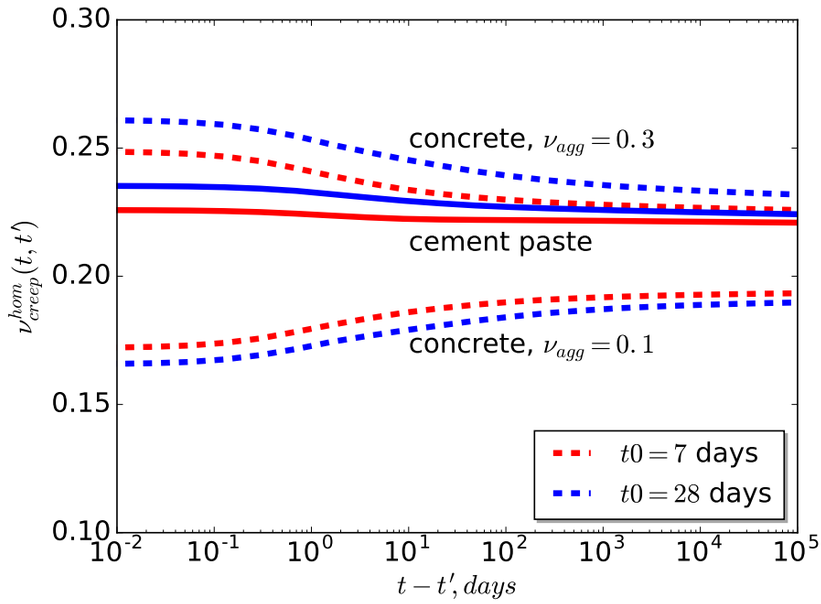

Figure 2.8: The estimated creep Poisson ratio are plotted for a cement paste (w/c=0.5) and two concretes (a/c=5.5) made of two aggregates featuring different Poisson ratio. Two ages at loading are considered: $t' = 7$ days and $t' = 28$ days. Both aggregates feature a Young modulus of 70GPa.

the issue. In addition, the admixtures, in particular retarders and water reducers, or the alkali content may affect the advance of hydration reactions and the mechanical properties of the concrete evolves rapidly at early age.

- Both the instantaneous strains and the basic creep strains of concretes featuring a small slump (< 40 mm, S1 class according to EN206-1) are underestimated. It might be due to particular air contents or difficulties in casting samples for creep tests. Accounting for the Young Modulus at the time of loading resolves the issue.

- The model can be applied to any aggregate to cement ratio. Nevertheless, soft aggregates are expected to induce larger creep strains. If the density or mineralogy of the aggregates significantly differs from normal aggregates, the stiffness of the aggregate must be accounted for. In addition, it must be recalled that the homogenization model assumes a perfect bonding between the aggregates and the cementitious matrix. Finally, it could be suggested to account for viscous recycled concrete aggregates by applying the model twice.

The temperature affects the time dependent strains in different ways. On the one hand, it accelerates the hydration of the cement: that phenomenon is already introduced in the hydration model. On the other hand, the temperature affects the compliance of the constitutive phases. This phenomenon can be accounted for by introducing an activation energy E_a such that $E_a/R = 5000$K, where $R \approx 8.314$J.mol^{-1}.K^{-1} is the ideal gas constant. Such activation energies are roughly comparable to those of hydration kinetics and a single equivalent time is often considered so as to ease the computations. Finally, increasing temperature increases the magnitude of creep strains to the point that time-temperature shift may not be relevant, thus preventing the use of high temperature to speed up creep tests on concrete. The proposed model only accounts for temperature through an activation energy of and it must therefore be limited to low and moderate temperature (5°C – 40°C). A temperature dependence arise from the microprestress theory, thus enabling the modelling of higher temperatures. Nevertheless, temperature not only affects the compliances of concretes, but also their elastic stiffness and strength and these effects are attributed to changes of nature, density or morphology of the hydration products. The proposed model might be able to account for these changes by introducing different C–S–H phases, which would solidify or dissolve depending on the temperature history.

Finally, it must be acknowledged that any chemical reaction consuming a load-bearing reactant would induce additional creep strains according to the proposed model. It clearly implies that estimating the creep strains of structures exposed to aggressive environments

and made of permeable concrete remains a challenging task.

3. Conclusion

A versatile and accurate modelling of the aging compliance of cementitious material is obtained by coupling a hydration model and mean-field schemes recently extended to aging linear viscoelasticity. The compliances of different phases of the cement paste are set according to nano-indentation results. Two types of C–S–H are introduced to account for the effect of relative humidity on basic creep strains. Hence, drying is modelled as a shift from wet C–S–H to dry C–S–H. Furthermore, a necessary drying creep arises from this shift and its magnitude is comparable to experimental values if and only if the shift induces significant changes of the stress field in the C–S–H gel, by means of a serial solidification compliance.

The model proved valuable to estimate the basic creep of concretes in situations where its composition is well-known. In addition, comparing the estimated strains for basic creep to those measured and gathered in the NU database proved interesting, as erroneous estimates were often triggered by wrong of missing details on the concrete. Unlike existing models of creep strains, the proposed model does not make use of the compressive strength of concrete. Nevertheless, the measured or prescribed compressive strength or Young modulus at the time of loading can be accounted for to correct the estimated creep strains. Finally, the advance of hydration at the age of loading prevails as the major source of uncertainty, in particular if the cement is sparsely described by its type. Accounting for the stiffness and density of the aggregate also improve the accuracy of the estimated creep strains.

Since the long-term logarithmic trend of basic creep is introduced at the scale of the C–S–H gel, the estimated creep strain of the concrete also features this trend. Nevertheless, the part of creep strains induced by the hydration, related to the dissolution of the clinker, is significant, especially for concretes featuring a high w/c ratio or loaded at early age. Samples stored in water may also feature a creep strain related to further hydration, change of internal relative humidity or lixiviation. The authors are convinced that most of chemical changes potentially occurring in concrete, such as lixiviation, carbonation or formation of Friedel's salt, may induce additional creep strains related to the dissolution of the load-bearing reactant. Therefore understanding and predicting the long-term creep strains of actual structures will likely remain a complex challenge since these processes may last for decades.

The present study is devoted to basic creep, but the model offers interesting perspectives regarding the modelling of drying creep, providing that the shape of the structure and its environmental conditions are accounted for in a practical way. The proposed model could be extended to shrinkage by taking account of the effect of capillary pressure [93, 94, 95]. These internal pressures would act as a tensile stress on the surface of water-filled capillary pores [93, 94]. Indeed, it can reasonably be assumed that the capillary pressure is balanced by the disjoining pressure in the adsorbed water film on the pore wall [94]. Similarly, a crystal growth pressure could be introduced as an eigenstress within the hydrates or at the scale of C-S-H, so as to explain swelling of concrete samples stored in water [93, 96]. If such a model proves accurate, a complete and versatile estimate of the time-dependent strains of concrete could be achieved.

Appendix A. A crude model for the pore size distribution of cement pastes

The modelled pore size distribution is designed to relate the water content to a relative humidity through a water diameter upon desiccation. It must be distinguished from the actual size of pores in the cement paste, as the sorption isotherm can be different from the desorption isotherm, showing the magnitude of the ink-bottle phenomenon [97, 93, 98]. The hydration model [1] considered in the present article is similar to HYMOSTRUCT [99] regarding this pore size distribution: the volume of capillary pores smaller than a diameter d varies directly with the logarithm of that diameter. On the contrary, mercury intrusion porosimetry unveils a bimodal distribution of capillary pores [100]. It describes the pore size distribution of pores of water diameter larger than 4.8nm, emptied at 65%RH as the pressure of mercury was limited to 300MPa. While accounting for this feature does not seem critical to hydration modelling, it may improve the estimate of the internal relative humidity, which directly affects the creep strains. The diameter reported in [100] are converted to mercury pressure using the third equation of that reference. Then a corresponding water diameter upon desiccation d is computed according to [93]: the mercury intrusion porosimetry test actually corresponds to the water desorption isotherm according to the ink-bottle phenomenon [93, 98]. As advised in

[101], the resulting cumulative pore size distributions are adjusted as a sum of two cumulative distribution functions of lognormal distributions:

$$c(d) = \frac{1}{2}c_s\left(1 + \text{erf}\left(\frac{\log(d) - \log(d_s)}{\sqrt{2}\sigma_s}\right)\right) + \frac{1}{2}(1 - c_s)\left(1 + \text{erf}\left(\frac{\log(d) - \log(d_b)}{\sqrt{2}\sigma_b}\right)\right) \quad \text{(A.1)}$$

where the fraction of small pores c_s, their characteristic diameter d_s, their size dispersion σ_s, the characteristic diameter of the big pores d_b and the corresponding dispersion σ_b are parameters to be adjusted. Finally, empirical expressions are built to estimate these parameters. The dispersion of big pores is found globally independent from the porosity and it is set to $\sigma_b = 0.4$. The fraction of small capillary pores decreases with the porosity ϕ_C representing the total volume of the capillary pores dried at 40% RH:

$$c_s = \begin{cases} 1 & \phi < 0.3 \\ 1 - \frac{2}{3}(\phi_C - 0.3)/(0.2) & \phi_C \geq 0.3 \text{ and } \phi_C \leq 0.6 \\ 0 & \phi \geq 0.6 \end{cases} \quad \text{(A.2)}$$

The characteristic diameter d_s (in m) of the small pores and the corresponding dispersion increase with the capillary porosity:

$$d_s = \begin{cases} 2 \times 10^{-8} & \phi_C < 0.15 \\ 2 \times 10^{-8} + 6 \times 10^{-8}(\phi_C - 0.15)/(0.45 - 0.15)\text{m} & \phi_C \geq 0.15 \text{ and } \phi_C \leq 0.45 \\ 8 \times 10^{-8} & \phi_C \geq 0.45 \end{cases} \quad \text{(A.3)}$$

$$\sigma_s = \begin{cases} 0.7 & \phi_C < 0.15 \\ 0.7 + (1.3 - 0.7)(\phi_C - 0.15)/(0.45 - 0.15) & \phi_C \geq 0.15 \text{ and } \phi_C \leq 0.45 \\ 1.3 & \phi_C \geq 0.45 \end{cases} \quad \text{(A.4)}$$

The characteristic diameter (in m) of the big pores writes:

$$d_b = 2 \times 10^{-7} + 2 \times 10^{-6}\left(\frac{\phi_C - 0.3}{0.2}\right)^2 \quad \text{(A.5)}$$

The accuracy of the proposed model is displayed on figure A.1. By assuming that the pore size distribution is solely governed by the capillary porosity, matching the measured porosity curves at all water to cement ratio can hardly be achieved. Nevertheless, the pore size distribution is likely better modelled than in HYMOSTRUCT [99], where it is assumed to be a straight line in such a semi-logarithmic plot.

To estimate the relative humidity starting from the advance of hydration reactions and total amount of water, the amount of liquid free capillary water not dried above 40% RH ϕ_W is computed according to the molar composition $C_xSH_{2.7}$ [102, 63] where the stoichiometric coefficient 2.7 accounts for non-evaporable water and gel constrained water. The volume of this unconstrained liquid water is computed using a molar volume of 18cm^3/mol. Moreover, the volume of the capillary pores dried at 40% RH, including pores filled by air and steam due to the chemical shrinkage or drying, denoted ϕ_C, is computed by assuming the molar volume of $C_{1.7}SH_{2.7}$ to be equal to 89cm^3/mol, consistent with a density of 2.31 [63]. Then, the diameter of largest water-filled pore d is the only diameter such that $\phi_W = c(d)\phi_C$. Finally, the relative humidity and capillary pressure are respectively computed by applying the Kelvin and Young-Laplace equations.

[1] F. Lavergne, A. B. Fraj, I. Bayane, J. Barthélémy, Estimating the mechanical properties of hydrating blended cementitious materials: An investigation based on micromechanics, Cement and Concrete Research ISSN 0008-8846, doi:10.1016/j.cemconres.2017.10.018, URL http://www.sciencedirect.com/science/article/pii/S0008884617304015.

[2] Z. P. Bažant, Mathematical models for creep and shrinkage of concrete, in: Z. P. Bažant, F. H. Wittmann (Eds.), Creep and shrinkage in concrete structures, Wiley Series in Numerical Methods in Engineering, chap. 7, Wiley, ISBN 9780471104094, 163 – 256, 1982.

[3] L. Granger, Comportement différé du béton dans les enceintes de centrales nucléaires : Analyse et modélisation, Ph.D. thesis, Ecole Nationale des Ponts et Chaussées, 1995.

[4] Z. Bazant, M. Jirásek, Creep and hygrothermal effects in concrete structures, IUTAM Bookseries 225 (2018) 1–45, ISSN 1875-3507, doi:10.1007/978-94-024-1138-6.

[5] Z. P. Bažant, S. Prasannan, Solidification Theory for Concrete Creep. I: Formulation, Journal of Engineering Mechanics 115 (8) (1989) 1691–1703, doi:10.1061/(ASCE)0733-9399(1989)115:8(1691), URL https://ascelibrary.org/doi/abs/10.1061/%28ASCE%290733-9399%281989%29115%3A8%281691%29.

[6] Z. P. Bazant, A. B. Hauggaard, S. Baweja, F.-J. Ulm, Microprestress-Solification Theory for concrete creep. I: Aging and Drying Effects, Journal of Engineering Mechanics 123 (11) (1997) 1188–1194, ISSN 0733-9399, doi:10.1061/(ASCE)0733-9399(1997)123:11(1188), URL https://doi.org/10.1061/(ASCE)0733-9399(1997)123:11(1188).

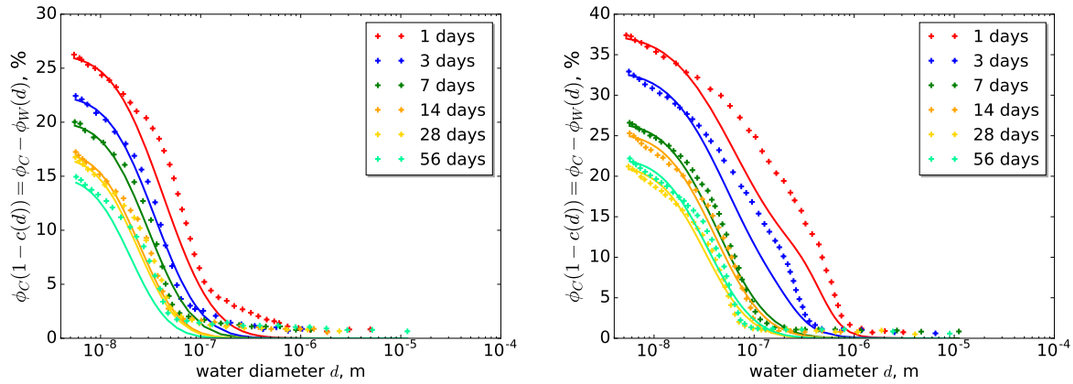

(a) $w/c = 0.3$

(b) $w/c = 0.4$

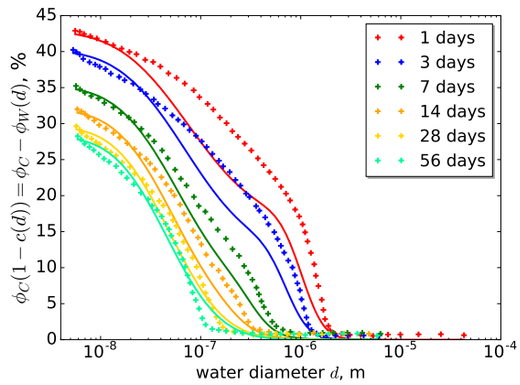

(c) $w/c = 0.5$

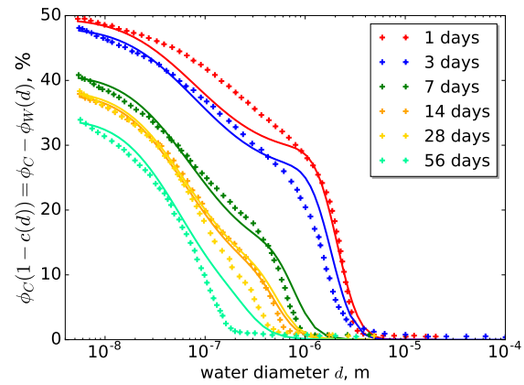

(d) $w/c = 0.6$

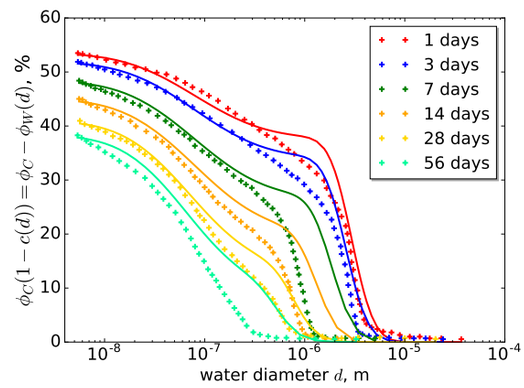

(e) $w/c = 0.7$

Figure A.1: The cumulative pore size distribution upon water desorption, converted from [100] (crosses) are compared to those obtained by applying the proposed model (lines).

[7] I. Pignatelli, A. Kumar, R. Alizadeh, Y. L. Pape, M. Bauchy, G. Sant, A dissolution-precipitation mechanism is at the origin of concrete creep in moist environments, The Journal of Chemical Physics 145 (5) (2016) 054701, doi:10.1063/1.4955429, URL `https://doi.org/10.1063/1.4955429`.

[8] M. Vandamme, The Nanogranular Origin of concrete creep: a nanoindentation investigation of microstructure and fundamental properties of Calcium-Silicate-Hydrates, Ph.D. thesis, Massachusetts Institute of Technology, 2008.

[9] M. Vandamme, F.-J. Ulm, Nanoindentation investigation of creep properties of calcium silicate hydrates, Cement and Concrete Research 52 (Supplement C) (2013) 38 – 52, ISSN 0008-8846, doi:10.1016/j.cemconres.2013.05.006, URL `http://www.sciencedirect.com/science/article/pii/S0008884613001191`.

[10] Q. Zhang, Propriétés mécaniques des matériaux cimentaires: effet de l'eau et de la microstructure, une approche par microindentation, Ph.D. thesis, Université Paris-Est, 2014.

[11] D.-T. Nguyen, Microindentation creep of Calcium-Silicate-Hydrate and secondary hydrated cement systems, Ph.D. thesis, University of Ottawa, 2014.

[12] Z. P. Bazant, S. Baweja, Creep and Shrinkage Prediction Model for Analysis and Design of Concretetructures: Model B3, Tech. Rep., American Concrete Institute, doi:10.14359/9889, URL `https://doi.org/10.14359/9889`, 2000.

[13] R. Wendner, M. H. Hubler, Z. P. Bažant, The B4 Model for Multi-decade Creep and Shrinkage Pre-

diction, in: Mechanics and Physics of Creep, Shrinkage, and Durability of Concrete, 429–436, doi:10.1061/9780784413111.051, URL https://ascelibrary.org/doi/abs/10.1061/9780784413111.051, 2013.

[14] Fédération internationale du béton, fib Model Code for Concrete Structures 2010, Wiley, ISBN 9783433604083, URL https://books.google.fr/books?id=rXUjAQAAQBAJ, 2013.

[15] J. A. Hanson, A 10-year study of creep properties of concrete, Tech. Rep. SP-38, Engineering Laboratories Branch, Design and Construction Division, Bureau of Reclamation, Denver, 1953.

[16] J. E. McDonald, Time-dependent deformation of concrete under multiaxial stress conditions, Tech. Rep. C-75-4, U. S. Army Engineer Waterways Experiment Station Concrete Laboratory, 1975.

[17] R. Le Roy, F. Le Maou, J. M. Torrenti, Long term basic creep behavior of high performance concrete: data and modelling, Materials and Structures 50 (2017) 11p, doi:10.1617/s11527-016-0948-8, URL https://hal.archives-ouvertes.fr/hal-01430831.

[18] J.-M. Torrenti, R. Le Roy, Analysis of some basic creep tests on concrete and their implications for modeling, Structural Concrete 19 (2) (2018) 483–488, doi:10.1002/suco.201600197, URL https://onlinelibrary.wiley.com/doi/abs/10.1002/suco.201600197.

[19] O. Bernard, F.-J. Ulm, E. Lemarchand, A multiscale micromechanics-hydration model for the early-age elastic properties of cement-based materials, Cement and Concrete Research 33 (9) (2003) 1293 – 1309, ISSN 0008-8846, doi:10.1016/S0008-8846(03)00039-5, URL http://www.sciencedirect.com/science/article/pii/S0008884603000395.

[20] G. Constantinides, F.-J. Ulm, The effect of two types of C-S-H on the elasticity of cement-based materials: Results from nanoindentation and micromechanical modeling, Cement and Concrete Research 34 (1) (2004) 67 – 80, ISSN 0008-8846, doi:10.1016/S0008-8846(03)00230-8, URL http://www.sciencedirect.com/science/article/pii/S0008884603002308.

[21] J. Sanahuja, L. Dormieux, G. Chanvillard, Modelling elasticity of a hydrating cement paste, Cement and Concrete Research 37 (10) (2007) 1427 – 1439, ISSN 0008-8846, doi:10.1016/j.cemconres.2007.07.003, URL http://www.sciencedirect.com/science/article/pii/S0008884607001548.

[22] S. Ghabezloo, Association of macroscopic laboratory testing and micromechanics modelling for the evaluation of the poroelastic parameters of a hardened cement paste, Cement and Concrete Research 40 (8) (2010) 1197 – 1210, ISSN 0008-8846, doi:10.1016/j.cemconres.2010.03.016, URL http://www.sciencedirect.com/science/article/pii/S0008884610000852.

[23] B. Pichler, C. Hellmich, Upscaling quasi-brittle strength of cement paste and mortar: A multi-scale engineering mechanics model, Cement and Concrete Research 41 (5) (2011) 467 – 476, ISSN 0008-8846, doi:10.1016/j.cemconres.2011.01.010, URL http://www.sciencedirect.com/science/article/pii/S0008884611000111.

[24] P. Termkhajornkit, Q. H. Vu, R. Barbarulo, S. Daronnat, G. Chanvillard, Dependence of compressive strength on phase assemblage in cement pastes: Beyond gel–space ratio — Experimental evidence and micromechanical modeling, Cement and Concrete Research 56 (2014) 1 – 11, ISSN 0008-8846, doi:10.1016/j.cemconres.2013.10.007, URL http://www.sciencedirect.com/science/article/pii/S0008884613002160.

[25] J. Sanahuja, Impact de la morphologie structurale sur les performances mécaniques des matériaux de construction : application au plâtre et à la pâte de ciment, Ph.D. thesis, Ecole Nationale des Ponts et Chaussées, 2008.

[26] C. Pichler, R. Lackner, A multiscale creep model as basis for simulation of early-age concrete behavior, Computers and Concrete 5 (4) (2008) 295 – 328, doi:10.12989/cac.2008.5.4.295, URL https://doi.org/10.12989/cac.2008.5.4.295.

[27] L. Göbel, M. Königsberger, A. Osburg, B. Pichler, Viscoelastic Behavior of Polymer-Modified Cement Pastes: Insight from Downscaling Short-Term Macroscopic Creep Tests by Means of Multiscale Modeling, Applied Sciences 8 (4), ISSN 2076-3417, doi:10.3390/app8040487, URL http://www.mdpi.com/2076-3417/8/4/487.

[28] Q. H. Do, Modelling properties of cement paste from microstructure: porosity, mechanical properties, creep and shrinkage, Ph.D. thesis, Ecole Polytechnique Fédérale de Lausanne, 2013.

[29] V. Šmilauer, Z. P. Bažant, Identification of viscoelastic C-S-H behavior in mature cement paste by FFT-based homogenization method, Cement and Concrete Research 40 (2) (2010) 197 – 207, ISSN 0008-8846, doi:10.1016/j.cemconres.2009.10.003, URL http://www.sciencedirect.com/science/article/pii/S0008884609002865.

[30] F. Lavergne, K. Sab, J. Sanahuja, M. Bornert, C. Toulemonde, Investigation of the effect of aggregates' morphology on concrete creep properties by numerical simulations, Cement and Concrete Research 71 (2015) 14 – 28, ISSN 0008-8846, doi:http://dx.doi.org/10.1016/j.cemconres.2015.01.003, URL http://www.sciencedirect.com/science/article/pii/S0008884615000101.

[31] J. Sanahuja, Effective behaviour of ageing linear viscoelastic composites: Homogenization approach, International Journal of Solids and Structures 50 (19) (2013) 2846 – 2856, ISSN 0020-7683, doi:10.1016/j.ijsolstr.2013.04.023, URL http://www.sciencedirect.com/science/article/pii/S0020768313001807.

[32] F. Lavergne, K. Sab, J. Sanahuja, M. Bornert, C. Toulemonde, Homogenization schemes for aging linear viscoelastic matrix-inclusion composite materials with elongated inclusions, International Journal of Solids and Structures 80 (2016) 545 – 560, ISSN 0020-7683, doi:10.1016/j.ijsolstr.2015.10.014, URL http://www.sciencedirect.com/science/article/pii/S0020768315004308.

[33] F. Lavergne, K. Sab, J. Sanahuja, M. Bornert, C. Toulemonde, An approximate multiscale model for aging viscoelastic materials exhibiting time-dependent Poisson's ratio, Cement and Concrete Research 86 (2016) 42 – 54, ISSN 0008-8846, doi:https://doi.org/10.1016/j.cemconres.2016.04.015, URL http://www.sciencedirect.com/science/article/pii/S0008884615300697.

[34] J.-F. Barthélémy, A. Giraud, F. Lavergne, J. Sanahuja, The Eshelby inclusion problem in ageing linear viscoelasticity, International Journal of Solids and Structures 97-98 (2016) 530 – 542, ISSN 0020-7683, doi:10.1016/j.ijsolstr.2016.06.035, URL http://www.sciencedirect.com/science/article/pii/S0020768316301500.

[35] J. Sanahuja, Efficient Homogenization of Ageing Creep of Random Media: Application to Solid-

ifying Cementitious Materials, in: Mechanics and Physics of Creep, Shrinkage, and Durability of Concrete, 1–7, doi:10.1061/9780784413111.023, URL https://ascelibrary.org/doi/abs/10.1061/9780784413111.023, 2014.

[36] T. Honorio, B. Bary, F. Benboudjema, Multiscale estimation of ageing viscoelastic properties of cement-based materials: A combined analytical and numerical approach to estimate the behaviour at early age, Cement and Concrete Research 85 (2016) 137 – 155, ISSN 0008-8846, doi:10.1016/j.cemconres.2016.03.010, URL http://www.sciencedirect.com/science/article/pii/S0008884615301411.

[37] T. Honorio, B. Bary, J. Sanahuja, Effective ageing linear viscoelastic properties of composites with phase precipitation: comparison between numerical and analytical homogenization approaches, in: 9th International Conference on Fracture Mechanics of Concrete and Concrete Structures, 1–8, URL http://framcos.org/FraMCoS-9/Full-Papers/228.pdf, 2016.

[38] J. Sanahuja, S. Huang, Mean-Field Homogenization of Time-Evolving Microstructures with Viscoelastic Phases: Application to a Simplified Micromechanical Model of Hydrating Cement Paste, Journal of Nanomechanics and Micromechanics 7 (1) (2017) 04016011, doi:10.1061/(ASCE)NM.2153-5477.0000116, URL 10.1061/(ASCE)NM.2153-5477.0000116.

[39] Z. P. Bažant, G.-H. Li, Comprehensive Database on Concrete Creep and Shrinkage, ACI Materials Journal 105 (2008) 1–12, doi:10.14359/20206, URL https://www.concrete.org/publications/internationalconcreteabstractsportal/m/details/id/20206.

[40] M. H. Hubler, R. Wendner, Z. P. Bažant, Comprehensive database for concrete creep and shrinkage: Analysis and recommendations for testing and recording, ACI Materials Journal 112 (4) (2015) 547–558, ISSN 0889-325X, doi:10.14359/51687452.

[41] NU Database of Laboratory Creep and Shrinkage Data, www.civil.northwestern.edu/people/bazant/CreepShrinkData_20180924GB.xlsx, accessed: 2018-11-12, 2018.

[42] S. Maghous, G. Creus, Periodic homogenization in thermoviscoelasticity: case of multilayered media with ageing, International Journal of Solids and Structures 40 (4) (2003) 851 – 870, ISSN 0020-7683, doi:10.1016/S0020-7683(02)00549-8, URL http://www.sciencedirect.com/science/article/pii/S0020768302005498.

[43] J.-F. Barthélémy, A. Giraud, J. Sanahuja, I. Sevostianov, Effective properties of ageing linear viscoelastic media with spheroidal inhomogeneities, International Journal of Engineering Science 144 (2019) 103104, ISSN 0020-7225, doi:https://doi.org/10.1016/j.ijengsci.2019.05.015, URL http://www.sciencedirect.com/science/article/pii/S0020722519309620.

[44] Z. Bažant, Numerical determination of long-range stress history from strain history in concrete, Matériaux et Construction 5 (3) (1972) 135–141, ISSN 0025-5432, doi:10.1007/BF02539255, URL http://dx.doi.org/10.1007/BF02539255.

[45] C. Huet, Adaptation d'un algorithme de Bazant au calcul des multilames visco-élastiques vieillissants, Matériaux et Construction 13 (2) (1980) 91–98, ISSN 1871-6873, doi:10.1007/BF02473805, URL http://dx.doi.org/10.1007/BF02473805.

[46] G. Constantinides, F.-J. Ulm, The nanogranular nature of C–S–H, Journal of the Mechanics and Physics of Solids 55 (1) (2007) 64 – 90, ISSN 0022-5096, doi:https://doi.org/10.1016/j.jmps.2006.06.003, URL http://www.sciencedirect.com/science/article/pii/S0022509606001062.

[47] Y. Bu, C. Saldana, C. Handwerker, J. Weiss, The Role of Calcium Hydroxide in the Elastic and Viscoelastic Response of Cementitious Materials: A Nanoindentation and SEM-EDS Study, in: K. Sobolev, S. P. Shah (Eds.), Nanotechnology in Construction: Proceedings of NICOM5, Springer International Publishing, Cham, ISBN 978-3-319-17088-6, 25–34, doi:10.1007/978-3-319-17088-6_3, URL https://doi.org/10.1007/978-3-319-17088-6_3, 2015.

[48] L. Sorelli, D. Pham, D. Vallée, J. Chen, M. Fafard, Finite Element Based Characterization of the creep properties of the cement paste phases by coupling nanoindentation technique and SEM-EDS, in: Mechanics and Physics of Creep, Shrinkage and Durability of Concrete: A Tribute to Zdeněk Bažant, 182–189, 2013.

[49] J. Salençon, Viscoélasticité pour le calcul des structures, Editions de l'Ecole Polytechnique, ISBN 978-2-7302-1557-2, 2016.

[50] A. B. Giorla, C. F. Dunant, Microstructural effects in the simulation of creep of concrete, Cement and Concrete Research 105 (2018) 44 – 53, ISSN 0008-8846, doi:10.1016/j.cemconres.2017.12.001, URL http://www.sciencedirect.com/science/article/pii/S000888461730488X.

[51] F. Bernachy-Barbe, B. Bary, Effect of aggregate shapes on local fields in 3D mesoscale simulations of the concrete creep behavior, Finite Elements in Analysis and Design 156 (2019) 13 – 23, ISSN 0168-874X, doi:https://doi.org/10.1016/j.finel.2019.01.001, URL http://www.sciencedirect.com/science/article/pii/S0168874X18306073.

[52] M. Vandamme, F.-J. Ulm, Nanogranular origin of concrete creep, Proceedings of the National Academy of Sciences 106 (26) (2009) 10552–10557, ISSN 0027-8424, doi:10.1073/pnas.0901033106, URL http://www.pnas.org/content/106/26/10552.

[53] M. Bauchy, E. Masoero, F.-J. Ulm, R. Pellenq, Creep of Bulk C-S-H: Insights from Molecular Dynamics Simulations, in: CONCREEP 10, 511–516, doi:10.1061/9780784479346.061, URL https://ascelibrary.org/doi/abs/10.1061/9780784479346.061, 2015.

[54] F. Wittmann, Einfluß des Feuchtigkeitsgehaltes auf das Kriechen des Zementsteines, Rheologica Acta 9 (2) (1970) 282–287, ISSN 1435-1528, doi:10.1007/BF01973489, URL https://doi.org/10.1007/BF01973489.

[55] S. Pihlajavaara, A review of some of the main results of a research on the ageing phenomena of concrete: Effect of moisture conditions on strength, shrinkage and creep of mature concrete, Cement and Concrete Research 4 (5) (1974) 761 – 771, ISSN 0008-8846, doi:https://doi.org/10.1016/0008-8846(74)90048-9, URL http://www.sciencedirect.com/science/article/pii/0008884674900489.

[56] Z. P. Bažant, A. A. Asghari, J. Schmidt, Experimental study of creep of hardened Portland cement paste at variable water content, Matériaux et Construction 9 (4) (1976) 279–290, ISSN 1871-6873, doi:10.1007/BF02478648, URL https://doi.org/10.1007/BF02478648.

[57] P. Acker, F.-J. Ulm, Creep and shrinkage of concrete: physical origins and practical measurements, Nuclear Engineering and Design 203 (2) (2001) 143 – 158, ISSN 0029-5493, doi:https:

//doi.org/10.1016/S0029-5493(00)00304-6, URL http://www.sciencedirect.com/science/article/pii/S0029549300003046.

[58] F. Benboudjema, Modelisation des déformations différées du béton sous sollicitations biaxiales. Application aux enceintes de confinement de batiments reacteurs des centrales nucléaires, Ph.D. thesis, Université de Marne la Vallée, 2002.

[59] A. Neville, A. Neville, Properties of Concrete, Pearson, ISBN 9780273755807, URL https://books.google.fr/books?id=vsztgAEACAAJ, 2011.

[60] F. Benboudjema, F. Meftah, J. Torrenti, Interaction between drying, shrinkage, creep and cracking phenomena in concrete, Engineering Structures 27 (2) (2005) 239 – 250, ISSN 0141-0296, doi:10.1016/j.engstruct.2004.09.012, URL http://www.sciencedirect.com/science/article/pii/S0141029604003359.

[61] Z. P. Bazant, J. C. Chern, Concrete creep at variable humidity: constitutive law and mechanism, Materials and Structures 18 (1) (1985) 1, ISSN 1871-6873, doi:10.1007/BF02473360, URL https://doi.org/10.1007/BF02473360.

[62] P. Acker, Swelling, shrinkage and creep: a mechanical approach to cement hydration, Materials and Structures 37 (4) (2004) 237–243, ISSN 1871-6873, doi:10.1007/BF02480632, URL https://doi.org/10.1007/BF02480632.

[63] H. M. Jennings, Refinements to colloid model of C-S-H in cement: CM-II, Cement and Concrete Research 38 (3) (2008) 275 – 289, ISSN 0008-8846, doi:https://doi.org/10.1016/j.cemconres.2007.10.006, URL http://www.sciencedirect.com/science/article/pii/S0008884607002761.

[64] L. Stefan, F. Benboudjema, F. Lagier, J. Torrenti, Percolation and creep of concrete at very early age behaviour, in: Creep, Shrinkage and Durability Mechanics of concrete and concrete structures, 169–175, 2009.

[65] B. T. Tamtsia, J. J. Beaudoin, J. Marchand, The early age short-term creep of hardening cement paste: load-induced hydration effects, Tech. Rep. NRCC-45703, Institute for Research in Construction, National Research Council of Canada, 2004.

[66] J. J. Beaudoin, B. T. Tamtsia, Creep of Hardened Cement Paste—The Role of Interfacial Phenomena, Interface Science 12 (4) (2004) 353–360, ISSN 1573-2746, doi:10.1023/B:INTS.0000042333.19983.3f, URL https://doi.org/10.1023/B:INTS.0000042333.19983.3f.

[67] B. Persson, Quasi-instantaneous and long-term deformations of high-performance concrete with some related properties, Tech. Rep. TVBM-1016, Division of Building Materials, Lund University, 1998.

[68] J. J. Brooks, 30-year creep and shrinkage of concrete, Magazine of Concrete Research 57 (9) (2005) 545–556, doi:10.1680/macr.2005.57.9.545, URL https://doi.org/10.1680/macr.2005.57.9.545.

[69] G. P. York, T. W. Kennedy, E. S. Perry, Experimental investigation of creep in concrete subjected to multiaxial compressive stresses and elevated temperatures, Tech. Rep. 2864-2, Departement of civil engineering, the University of Texas, 1970.

[70] R. Le Roy, Déformations instantanées et différées des bétons à hautes performances, Ph.D. thesis, Ecole Nationale des Ponts et Chaussées, 1995.

[71] P. Laplante, Propriétés mécaniques des bétons durcissants : analyse comparée des bétons classiques et à très hautes performances, Tech. Rep. série Ouvrages d'art, Laboratoire Central des Ponts et Chaussées, URL http://www.ifsttar.fr/fileadmin/user_upload/editions/lcpc/ERLPC/ERLPC-OA-LCPC-OA13.pdf, 1993.

[72] ACI Committee 209, Guide for modeling and calculating Shrinkage and creep in hardened concrete, Tech. Rep. ACI 209.2R-08, American Concrete Institute, 2008.

[73] J. R. Keeton, Creep and shrinkage of reinforced thin-shell concrete, Tech. Rep. R-704, Naval Civil Engineering Laboratory, Port Hueneme, California, 1970.

[74] J. R. Evans, T. P. Anderson, M. W. Manson, R. L. Maud, W. B. Clark, D. L. Fife, Aggregates in the greater Los Angeles Area, California, Tech. Rep. Special report 139, California Division of Mines and Geology, 1979.

[75] R. D. Browne, R. Blundell, The influence of loading age and temperature on the long term creep behaviour of concrete in a sealed, moisture stable, state, Matériaux et Construction 2 (2) (1969) 133–143, ISSN 1871-6873, doi:10.1007/BF02475101, URL https://doi.org/10.1007/BF02475101.

[76] R. Browne, PROPERTIES OF CONCRETE IN REACTOR VESSELS., pp 131-51 of Prestressed Concrete Pressure Vessels. Udall, Marilyn S. (ed.). London, Institution of Civil Engineers, 1968. .

[77] R. Browne, R. Blundell, The behaviour of concrete in prestressed concrete pressure vessels, Nuclear Engineering and Design 20 (2) (1972) 429 – 475, ISSN 0029-5493, doi:https://doi.org/10.1016/0029-5493(72)90123-9, URL http://www.sciencedirect.com/science/article/pii/0029549372901239.

[78] R. K. Nanstad, A review of concrete properties for prestressed concrete pressure vessels, Tech. Rep. ORNL/TM-5497, Oak Ridge National Laboratory, 1976.

[79] L. M. Maia, S. Nunes, J. A. Figueiras, Influence of paste content on shrinkage and creep of SCC, in: Creep, Shrinkage and Durability mechanics of concrete and concrete structures, 675–680, 2009.

[80] B. Persson, A comparison between mechanical properties of self-compacting concrete and the corresponding properties of normal concrete, Cement and Concrete Research 31 (2) (2001) 193 – 198, ISSN 0008-8846, doi:https://doi.org/10.1016/S0008-8846(00)00497-X, URL http://www.sciencedirect.com/science/article/pii/S000888460000497X.

[81] J. J. Brooks, A. M. Neville, Estimating long-term creep and shrinkage from short-term tests, Magazine of Concrete Research 27 (90) (1975) 3–12, doi:10.1680/macr.1975.27.90.3, URL https://doi.org/10.1680/macr.1975.27.90.3.

[82] M. Mamillan, Evolution du fluage et des propriétés du béton, Annales de l'Institut Technique du Bâtiment et des Travaux Publics 154 (1960) 1017–1077.

[83] N. Tue, J. Ma, M. Orgass, Kriechen von Ultrahochfestem Beton (UHFB), Bautechnik 83 (2) (2006) 119–124, doi:10.1002/bate.200610012, URL https://onlinelibrary.wiley.com/doi/abs/10.1002/bate.200610012.

[84] E. C. for Standardization, EN 1992-1-1 Eurocode 2: Design of concrete structures - Part 1-1: General ruels and rules for buildings, Tech. Rep. EN 1992-1-1:2004, EN, 2004.

[85] E. C. for Standardization, EN 1992-2 Eurocode 2: Design of concrete structures - Part 2: Concrete

bridges - design and detailing rules, Tech. Rep. EN 1992-2:2005, EN, 2005.

[86] N. J. Gardner, Comparison of prediction provisions for drying shrinkage and creep of normal-strength concretes, Canadian Journal of Civil Engineering 31 (5) (2004) 767–775, doi:10.1139/l04-046, URL https://doi.org/10.1139/l04-046.

[87] RILEM, RILEM draft recommendation: TC-242-MDC multi-decade creep and shrinkage of concrete: material model and structural analysis, Tech. Rep. TC-242-MDC, RILEM, doi:10.1617/s11527-014-0485-2, 2015.

[88] C. Famy, K. L. Scrivener, H. F. W. Taylor, Delayed ettringite formation, in: P. Barnes, J. Bensted (Eds.), Structure and Performance of Cements, chap. 10, CRC Press, ISBN 9781482295016, 282–294, URL https://www.crcpress.com/Structure-and-Performance-of-Cements-Second-Edition/Barnes-Bensted/p/book/9780419233305, 2014.

[89] T. Petersen, F.-J. Ulm, Phase-field modeling of cement paste: Where particle physics meets continuum mechanics, in: G. Meschke, B. Pichler, J. Rots (Eds.), Computational Modelling of Concrete Structures: Proceedings of the Conference on Computational Modelling of Concrete and Concrete Structures (EURO-C 2018), February 26 - March 1, 2018, Bad Hofgastein, Austria, CRC Press, ISBN 9781351726764, 79–86, URL https://www.taylorfrancis.com/books/e/9781351726764/chapters/10.1201%2F9781315182964-8, 2018.

[90] X. Li, Z. Grasley, J. Bullard, E. Garboczi, Computing the time evolution of the apparent viscoelastic/viscoplastic Poisson's ratio of hydrating cement paste, Cement and Concrete Composites 56 (2015) 121 – 133, ISSN 0958-9465, doi:https://doi.org/10.1016/j.cemconcomp.2014.11.004, URL http://www.sciencedirect.com/science/article/pii/S0958946514002078.

[91] J. K. Kim, S. H. Kwon, S. Y. Kim, Y. Y. Kim, Experimental studies on creep of sealed concrete under multiaxial stresses, Magazine of Concrete Research 57 (10) (2005) 623–634, doi:10.1680/macr.2005.57.10.623, URL https://doi.org/10.1680/macr.2005.57.10.623.

[92] L. Charpin, Y. L. Pape, E. Coustabeau, B. Masson, J. Montalvo, EDF Study of 10-Year Concrete Creep under Unidirectional and Biaxial Loading: Evolution of the Poisson Coefficient under Sealed and Unsealed Conditions, 1381–1390, doi:10.1061/9780784479346.163, URL https://ascelibrary.org/doi/abs/10.1061/9780784479346.163, 2015.

[93] C. Pichler, R. Lackner, H. A. Mang, A multiscale micromechanics model for the autogenous-shrinkage deformation of early-age cement-based materials, Engineering Fracture Mechanics 74 (1) (2007) 34 – 58, ISSN 0013-7944, doi:10.1016/j.engfracmech.2006.01.034, URL http://www.sciencedirect.com/science/article/pii/S0013794406000464, fracture of Concrete Materials and Structures.

[94] S. F. Rahman, Z. C. Grasley, The significance of pore liquid pressure and disjoining pressure on the desiccation shrinkage of cementitious materials, International Journal of Advances in Engineering Sciences and Applied Mathematics 9 (2) (2017) 87–96, ISSN 0975-5616, doi:10.1007/s12572-017-0186-5, URL https://doi.org/10.1007/s12572-017-0186-5.

[95] A. Aili, M. Vandamme, J.-M. Torrenti, B. Masson, Is long-term autogenous shrinkage a creep phenomenon induced by capillary effects due to self-desiccation?, Cement and Concrete Research 108 (2018) 186 – 200, ISSN 0008-8846, doi:https://doi.org/10.1016/j.cemconres.2018.02.023, URL http://www.sciencedirect.com/science/article/pii/S0008884617309389.

[96] Z. P. Bažant, A. Donmez, E. Masoero, S. R. Aghdam, Interaction of Concrete Creep, Shrinkage and Swelling with Water, Hydration, and Damage: Nano-Macro-Chemo, in: CONCREEP 10, 1–12, doi:10.1061/9780784479346.001, URL https://ascelibrary.org/doi/abs/10.1061/9780784479346.001, 2015.

[97] F. Moro, H. Böhni, Ink-Bottle Effect in Mercury Intrusion Porosimetry of Cement-Based Materials, Journal of Colloid and Interface Science 246 (1) (2002) 135 – 149, ISSN 0021-9797, doi:https://doi.org/10.1006/jcis.2001.7962, URL http://www.sciencedirect.com/science/article/pii/S0021979701979627.

[98] Q. Zeng, D. Zhang, H. Sun, K. Li, Characterizing pore structure of cement blend pastes using water vapor sorption analysis, Materials Characterization 95 (2014) 72 – 84, ISSN 1044-5803, doi:10.1016/j.matchar.2014.06.007, URL http://www.sciencedirect.com/science/article/pii/S1044580314001739.

[99] K. van Breugel, Simulation of Hydration and Formation of Structure in Hardening Cement-Based Materials, Ph.D. thesis, T.U. Delft, 1991.

[100] R. A. Cook, K. C. Hover, Mercury porosimetry of hardened cement pastes, Cement and Concrete Research 29 (6) (1999) 933 – 943, ISSN 0008-8846, doi:10.1016/S0008-8846(99)00083-6, URL http://www.sciencedirect.com/science/article/pii/S0008884699000836.

[101] D. M. Roy, P. W. Brown, D. Shi, B. E. Scheetz, W. May, Concrete Microstructure Porosity and Permeability, Tech. Rep. SHRP-C-628, Strategic Highway Research Program, URL http://onlinepubs.trb.org/onlinepubs/shrp/shrp-c-628.pdf, 1993.

[102] J. J. Thomas, S. A. FitzGerald, D. A. Neumann, R. A. Livingston, State of Water in Hydrating Tricalcium Silicate and Portland Cement Pastes as Measured by Quasi-Elastic Neutron Scattering, Journal of the American Ceramic Society 84 (8) (2001) 1811–1816, doi:10.1111/j.1151-2916.2001.tb00919.x, URL https://ceramics.onlinelibrary.wiley.com/doi/abs/10.1111/j.1151-2916.2001.tb00919.x.

[103] J. Brooks, M. M. Johari, Effect of metakaolin on creep and shrinkage of concrete, Cement and Concrete Composites 23 (6) (2001) 495 – 502, ISSN 0958-9465, doi:10.1016/S0958-9465(00)00095-0, URL http://www.sciencedirect.com/science/article/pii/S0958946500000950, metakaolin and Calcined Clays.

[104] I. Anders, Stoffgesetz zur Beschreibung des Kriech- und Relaxationsverhaltens junger normal- und hochfester Betone, Ph.D. thesis, Karlsruher Instituts für Technologie, 2011.

[105] Y. Aoyagi, Y. Onuma, M. Kawasaki, Experimental Study on Behavior of Prestressed Concrete Beams under Temperature Gradient., Tech. Rep. 70003, Central Research Institute of Electric Power Industry, 1970.

[106] S. Arthanari, C. W. Yu, Creep of concrete under uniaxial and biaxial stresses at elevated temperatures, Magazine of Concrete Research 19 (60) (1967) 149–156, doi:10.1680/macr.1967.19.60.149, URL https://doi.org/10.1680/macr.1967.19.60.149.

[107] H. Asch, S. Stöckl, Wärmedehnung, E-Modul, Swinden, Kriechen und Restfestigkeit von Reaktorbeton unter einachsiger Belastung und erhöhten Temperaturen, Tech. Rep. Heft 324, Deutscher Ausschuss für

Stahlbeton, 1981.
[108] W. H. Dilger, C. Wang, K. Niitaki, Experimental study on shrinkage and creep of high performance concrete, in: 4th INTERNATIONAL SYMPOSIUM ON THE UTILIZATION OF HIGH STRENGTH HIGH PERFORMANCE CONCRETE, ISBN 2859782605, 311–320, 1996.
[109] R. Dutron, Deformations lentes du beton armé sous l'action des charges permanentes, Annales des Travaus Publics de Belgique 37 (2).
[110] D. J. Hannant, Strain behaviour of concrete up to 95°C under compressive stresses, 171–191, doi:10.1680/pcpv.44760.0020, URL https://www.icevirtuallibrary.com/doi/abs/10.1680/pcpv.44760.0020, 1968.
[111] R. Johansen, C. H. Best, Creep of concrete with and without ice in the system, RILEM Bulletin 16 (1962) 47–57.
[112] T. Kanazu, Y. Aoyagi, T. Nakano, Evaluation of Temperature Cracking Tendensies of Hardened Concrete Using Newly Developed Apparatus, Tech. Rep. 382049, Central Research Institute of Electric Power Industry, 1983.
[113] M. Kawasumi, K. Kasahara, T. Kuriyama, Creep of Concrete at Elevated Temperatures, Part 3, The Influence of Ages at Loading and Water/Cement Ratios, Tech. Rep. 382008, Central Research Institute of Electric Power Industry, 1982.
[114] G. J. KOMMENDANT, M. Polivka, D. Pirtz, Study of concrete properties for prestressed concrete reactor vessels, Tech. Rep. UCSESM 76-3, Dept. of Civil Eng., University of California, 1976.
[115] T. Kumono, S. Nishibayashi, T. Kuroda, Effect of sustained tensile stress on microstructure of concrete, in: JPA proceedings of Cement & Concrete, 51, 818–823, 1997.
[116] F. de Larrard, Formulation et propriétés des bétons à très hautes performances, Laboratoire Central des Ponts et Chaussées Paris: Rapport de recherche, Laboratoire central des ponts et chaussées, ISBN 9782720875809, 1988.
[117] Y. Lee, S.-T. Yi, M.-S. Kim, J.-K. Kim, Evaluation of a basic creep model with respect to autogenous shrinkage, Cement and Concrete Research 36 (7) (2006) 1268 – 1278, ISSN 0008-8846, doi:https://doi.org/10.1016/j.cemconres.2006.02.011, URL http://www.sciencedirect.com/science/article/pii/S000888460600041X.
[118] K.-H. Min, K.-Y. Kwon, Y. Kim, J.-M. Yang, Y.-S. Yoon, An experimental study on time-dependent behaviors of early-aged concrete in various curing environments, in: Creep, Shrinkage and Durability Mechanics of concrete and concrete structures, 387–393, 2009.
[119] V. Mossiossian, W. L. Gamble, Time-dependent behavior of noncomposite and composite prestressed concrete structures under field and laboratory conditions, Tech. Rep. UILU-ENG-72-2006, Dept. of Civil Eng., University of Illinois, 1972.
[120] J. Navrátil, Application of Extension of model B3 for Concrete creep and shrinkage prediction. (in Czech), Tech. Rep., Stavební obzor, v tisku, 1996.
[121] A. S. Ngab, A. H. Nilson, F. O. Slate, Shrinkage and Creep of High Strength Concrete, ACI Journal Proceedings 78 (4) (1981) 255–261, doi:10.14359/6922.
[122] H. Ohnuma, Y. Aoyagi, H. Abe, T. Okazawa, Experimental Study on Creep Behavior of Concrete under Sustained Temperature Gradient in a Model of Prestressed Concrete Reactor Structures, Tech. Rep. 379005, Central Research Institute of Electric Power Industry, 1979.
[123] H. Ohnuma, Y. Aoyagi, T. Kuriyama, Creep Characteristics of Expansive Concrete under Uiaxial Compressive Stresses., Tech. Rep. 382047, Central Research Institute of Electric Power Industry, 1983.
[124] K. Okada, H. Kasa, Y. Yoshioka, M. Sakuta, T. Sato, Creep of Concrete at Elevated Temperature, Tech. Rep. 17, Takenaka Technical Research report, 1983.
[125] T. Okajima, K. Ohiwa, S. Tsujino, N. Hasegawa, K. Okada, A. Yamase, Creep of Concrete subjected to multi-axial stresses, in: Transactions of the Architectural Institute of Japan, 242, 55–61, 1976.
[126] D. Pirtz, Creep Characteristics of mass concrete for Dworshak dam, Tech. Rep. 65-2, Dept. of Civil Eng., University of California, 1968.
[127] F. S. Rostary, K.-T. Teichen, H. Engelke, Beitrag zur Klärung des Zussammenhanges von Kriechen und Relaxation bei Normal- beton, Tech. Rep. Heft 139, Amtliche Forschungsund Materialprüfungsanstalt für das Bauwesen, 1972.
[128] H. G. Russell, A. E. Fiorato, High-Strength Concrete Research for Buildings and Bridges, ACI Special Publication 159 (1996) 375–392, doi:10.14359/1606.
[129] P. Schwesinger, G. Ehlert, R. Wölfel, Creep of concrete at elevated temperatures and boundary conditions of moisture, Cement and Concrete Research 17 (2) (1987) 263 – 272, ISSN 0008-8846, doi:https://doi.org/10.1016/0008-8846(87)90109-8, URL http://www.sciencedirect.com/science/article/pii/0008884687901098.
[130] S. Seki, M. Kawasumi, Creep of Concrete at Elevated Temperatures, ACI Special Publication 34 (1972) 591–638, doi:10.14359/18088.
[131] S. Shritharan, Structural Effects of Creep and Shrinkage on Concrete Structures, Ph.D. thesis, University of Auckland, 1989.
[132] H. Takahashi, T. Kawagushi, Study on Time-Dependent Behavior of High Strength Concrete (Part 1) - Application of the Time - Dependent Linear Viscoelasticity Theory of Concrete Creep Behavior, Tech. Rep. 21, Ohbayashi-Gumi Research Institute, 1980.
[133] H. Takahashi, T. Kawagushi, Study on Time-Dependent Behavior of High Strength Concrete (Part 2) - Results of Creep Tests of Concrete at Elevated Temperature, Tech. Rep. 23, Ohbayashi-Gumi Research Institute, 1981.
[134] Y. Theiner, M. Drexel, M. Neuner, G. Hofstetter, Comprehensive study of concrete creep, shrinkage, and water content evolution under sealed and drying conditions, Strain 53 (2) (2017) e12223, doi:10.1111/str.12223, URL https://onlinelibrary.wiley.com/doi/abs/10.1111/str.12223, e12223 STRAIN-1220.R1.
[135] G. E. Troxell, J. M. Raphael, R. E. Davis, Long-Time Creep and Shrinkage Tests of Plain and Reinforced Concrete, in: ASTM Proceeding, vol. 58, 1121–1142, 1958.